In vitro maturation of *Toxoplasma gondii* bradyzoites in human myotubes and their metabolomic characterization

Authors

Céline Christiansen[1], Deborah Maus[1], Ellen Hoppenz[1], Mateo Murillo-León[4,5,6], Tobias Hoffmann[2], Jana Scholz[1], Florian Melerowicz[1], Tobias Steinfeldt[4,5], Frank Seeber[3], Martin Blume[1,7 *]

1 NG2: Metabolism of Microbial Pathogens, Robert Koch-Institute, 13353, Berlin, Germany
2 ZBS 4: Advanced Light and Electron Microscopy, Centre for Biological Threats and Special Pathogens 4, Robert Koch-Institute, 13353, Berlin, Germany
3 FG 16: Mycotic and Parasitic Agents and Mycobacteria, Robert Koch-Institute, 13353, Berlin, Germany
4 Institute of Virology, Medical Center University of Freiburg, 79104 Freiburg, Germany.
5 Faculty of Medicine, University of Freiburg, 79104 Freiburg, Germany.
6 Faculty of Biology, University of Freiburg, 79104 Freiburg, Germany.
7 Lead contact
* Corresponding author

Martin Blume
Junior Group 2
Robert Koch-Institute
Seestr. 10
13353 Berlin
Germany
Email: blumem@rki.de

Abstract

The apicomplexan parasite *Toxoplasma gondii* forms bradyzoite-containing tissue cysts that cause chronic and drug-tolerant infections. However, current *in vitro* models do not allow long-term culture of these cysts to maturity. Here, we developed a human myotube-based *in vitro* culture model of functionally mature tissue cysts that are orally infectious to mice and tolerate exposure to a range of antibiotics and temperature stresses . Metabolomic characterization of purified cysts reveals global changes that comprise increased levels of amino acids and decreased abundance of nucleobase- and tricarboxylic acid cycle-associated metabolites. In contrast to fast replicating tachyzoite forms of *T. gondii* these tissue cysts tolerate exposure to the aconitase inhibitor sodium fluoroacetate. Direct access to persistent stages of *T. gondii* under defined cell culture conditions will be essential for the dissection of functionally important host-parasite interactions and drug evasion mechanisms. It will also facilitate the identification of new strategies for therapeutic intervention.

Introduction

Toxoplasma gondii is an apicomplexan parasite that infects most warm-blooded animals, including an estimated third of all humans[1]. Similar to other infectious protozoa, including the apicomplexan *Plasmodium vivax*, the kinetoplastidae *Trypanosoma cruzi* and *Leishmania* spp., *T. gondii* forms specialized persistent stages that resist immune responses and many medical treatments[2]. *T. gondii* bradyzoites reside, surrounded by a glycan-rich cyst wall, predominantly in brain and muscle tissue and can be transmitted through ingestion of undercooked meat products[3]. These largely asymptomatic infections can cause recurring disease in immune-weakened individuals that are lethal if untreated[4].

The rapid proliferation of tachyzoites and the slow replication or dormancy of bradyzoites exert distinct demands on the metabolism of *T. gondii*. The rate of proliferation and the metabolic state are closely interrelated. They have been shown to independently affect lethality of antibiotics against bacterial microbes, with metabolism being the dominant factor[5]. While multiple metabolomic investigations on the tachyzoite stage of *T. gondii* revealed unexpected features of key metabolic pathways such as the GABA-shunt of the tricarboxylic acid (TCA) cycle, a constitutively active gluconeogenic fructose 1,6-bisphosphatase and the presence of a non-oxidative pentose phosphate pathway[6-8], the metabolism of bradyzoites has only been characterized indirectly[9], largely due to experimental constraints. In contrast to tachyzoites, bradyzoites depend on the turnover of the storage polysaccharide amylopectin by glycogen phosphorylase[10], the hexose kinase[11] and on a dedicated isoform of lactate dehydrogenase[12]. This indicates that glycolytic degradation of glucose plays an important role in bradyzoites. Similarly, the relevance of mitochondrial and amino acid metabolism has been inferred. Bradyzoite formation is induced by a number of electron transport inhibitors, including atovaquone, rotenone, oligomycin and antimycin[13,14]. Moreover, *T. gondii* cysts survive extended atovaquone exposure *in vivo*[15-17], indicating that their mitochondrial electron transport chain is not strictly essential. Similarly, bradyzoites can also be induced by limiting supply of exogenous amino acids[14] and their viability depends on proteolysis in their plant-like vacuolar compartment[18] and on autophagy[19]. Collectively, these data indicate a substantial remodeling of metabolic homeostasis in bradyzoites as a strategy to cope with nutrient limitations[20]. This proposed metabolic shift may also be associated with tolerance against many antiparasitic treatments, as the metabolic state of microbes has important implications for the lethality of antimicrobials[5].

However, our ability to investigate such mechanisms remains very limited by the lack of adequate *in vitro* culture models[2]. Current methods to experimentally generate mature *T. gondii* tissue cysts are confined to murine infections with cystogenic *T. gondii* strains[21,22]. The number of obtainable cysts from this *in vivo* model is low, precluding their metabolic analysis with current mass spectrometry-based approaches. In contrast, *in vitro* models are scalable and the stage conversion of *T. gondii* can be induced by a variety of treatments, such as alkaline, heat and chemical stress[23], nutrient starvation[24], excess adenosine[25], inhibitors of parasite protein kinases[26] as well as host cell-dependent factors such as cell cycle arrest and low glycolytic flux[20,27,28]. In addition, the infection of C2C12 murine skeletal muscle cells,neurons[29,30] and primary murine brain cells[31] facilitates spontaneous stage conversion of cystogenic strains. Generally, maturation times of *in vitro* cysts remain brief, but cysts develop detectable tolerance against short exposure to low doses of pyrimethamine after three days[10] and become orally infectious to mice at high doses after five days of culture[32]. However, establishment of long-term cultures that allow development of pan-antimicrobial- and temperature stress-tolerant cysts[33,34] remains a challenge. Incomplete differentiation leads to expansion of proliferating parasite populations and subsequent host cell lysis that limits the scale and duration of current *in vitro* culture systems.

Here, we developed a human myotube-based *in vitro* culture system that is scalable and enables long-term maturation of *T. gondii* cysts. The cysts resemble *in vivo* cysts in their ultrastructure, tolerance to antiparasitics and temperature stress and infectiousness to mice. Mass spectrometry-based metabolic profiling revealed a distinct metabolome that renders tissue cysts insensitive towards the aconitase inhibitor sodium fluoroacetate (NaFAc).

Materials and Methods

Host cell lines and cultivation

All cultures were maintained in a 37 °C humidified CO_2 (10 %) incubator as described previously[7].

Briefly, human foreskin fibroblast (HFF) monolayers were cultured in Dulbecco's Modified Eagle's Medium (DMEM) (Gibco) supplemented with 25 mM glucose (Sigma-Aldrich), 4 mM L-glutamine (Thermo Fisher Scientific), 1 mM sodium pyruvate (Capricorn Scientific), 100 U/ml penicillin, 100 µg/ml streptomycin (Thermo Fisher Scientific) and 10 % heat-inactivated calf serum (Capricorn Scientific).

The immortalized human myoblast cell line KD3 (a kind gift of N. Hashimoto; [35]), initially derived from normal subcutaneous female muscle tissue, was cultured in DMEM supplemented with 25 mM glucose, 4 mM L-glutamine, 1 mM sodium pyruvate, 100 U/ml penicillin, 100 µg/ml streptomycin, 2 % Ultroser G (Cytogen GmbH) and 20 % heat inactivated fetal bovine serum (FBS) (Capricorn Scientific). The differentiation of myoblasts into myotubes was induced at 70 % confluency by changing medium to DMEM supplemented with 25 mM glucose, 4 mM L-glutamine, 1 mM sodium pyruvate, 100 U/ml penicillin, 100 µg/ml streptomycin, 2 % horse serum (HOS) (Capricorn Scientific), 10 µg/ml human insulin (Sigma-Aldrich), 5 µg/ml human holo-transferrin (PAN Biotech) and 1.7 ng/µl sodium selenite (Sigma-Aldrich) for five to seven days[35].

Parasite strains cultivation and differentiation

Type I strain RH[36], RH-*Δku80Δhxgprt* (RH*Δku80*)[37], GT1[38], Type II ME49[39], NTE[39], Pru-*Δku80Δhxgprt(BSG-4) (*Pru-GFP*)*[40], Pru-*Δhxgprt* tdTomato (Pru-tdTomato)[41] and Type III NED[42], VEG ([43], provided by G. Schares), were maintained *in vitro* in HFF monolayers grown in DMEM supplemented with 25 mM glucose, 4 mM L-glutamine, 1 mM sodium pyruvate, 100 U/ml penicillin, 100 µg/ml streptomycin and 1 % heat-inactivated FBS (tachyzoite medium). Freshly egressed parasites were passaged by transfer to new HFF monolayers.

Differentiation of tachyzoites into tissue cysts was facilitated by CO_2 depletion at pH 7.4 if not otherwise indicated. To avoid acidification, the medium was changed to low glucose (5 mM), 50 mM HEPES (Sigma-Aldrich) buffered Roswell Park Memorial Institute 1640 (RPMI) medium (Gibco) supplemented with 4 mM L-glutamine, 100 U/ml penicillin, 100 µg/ml streptomycin, 2 % HOS and 10 µg/ml human insulin, 5 µg/ml human holo-transferrin and 1.7 ng/µl sodium selenite

(bradyzoite medium). The cells were incubated at 37 °C and ambient CO_2 levels. Medium was changed every two days and cells were washed once per week with phosphate buffered saline (PBS). The day after infection, infected monolayers were washed with prewarmed PBS to remove not invaded parasites. Medium was changed every second day and bradyzoite cultures were washed with PBS once a week. For assays involving plate reader-based fluorescence measurements, phenol red was omitted from the medium.

Electron microscopy

KD3 myotube cultures in T60 dishes were infected with $1.3x10^6$ Pru-tdTomato tachyzoites corresponding to a multiplicity of infection (MOI) of 0.3 and bradyzoite formation was facilitated for the indicated times in bradyzoite medium at ambient CO_2 levels. On the day of the experiment, the medium was removed and samples were fixed by covering the monolayer with 1 % paraformaldehyde (Sigma-Aldrich) and 2.5 % glutaraldehyde (Sigma-Aldrich) in 0.05 M HEPES buffer (pH 7.4). After incubation at room temperature (RT) for 3 h, samples were sealed with parafilm and stored in the fridge until further processing.

For plastic embedding, cells were scraped off with a cell scraper, sedimented by centrifugation (3000 x *g*, 10 min) and washed twice with 0.05 M HEPES buffer for removing the fixative. The washed cell pellets were mixed with 3 % low-melting point agarose (1:1 [v/v]) at 40 °C, centrifuged (3000 x *g*, 5 min) and cooled on ice. The cell pellets were cut off from the agarose gel block using a sharp razor blade and stored in 2.5 % glutaraldehyde in 0.05 M HEPES buffer. Post-fixation, block contrasting and dehydration, embedding in epoxy resin was performed according to a standard procedure [44]. Ultrathin sections with a thickness of ~65 nm were generated with an ultramicrotome (UC7, Leica Microsystems, Germany) using a diamond knife (45°, Diatome), collected on copper slot grids and contrasted with 2 % uranyl acetate (Thermo Fisher Scientific) and 0.1 % lead citrate (Sigma-Aldrich).

Electron microscopy of ultrathin sections was performed with a transmission electron microscope (Tecnai Spirit, Thermo Fisher Scientific) at 120 kV. Images were recorded with a side-mounted CCD camera (Megaview III, EMSIS, Germany) and the montage function of the camera software (Multiple Image Alignment, iTEM; EMSIS) was used to cover larger field of views with sufficient pixel resolution.

Immunofluorescence assay

Uninfected host cells were grown in monolayers on 12 mm round glass coverslips (TPP) and infected for 24 h, unless indicated otherwise. For bradyzoite experiments, independent of strain and host cell background, myotube monolayers were infected with $1.3x10^4$ extracellular tachyzoites corresponding to an MOI of 0.1 and incubated for the indicated times. Samples were fixed with 4 % paraformaldehyde in PBS for 20 min at RT followed by a washing step in 0.1 M glycine/PBS (Thermo Fisher Scientific) and permeabilization for 20 min in 0.1 % Triton X-100 (Thermo Fisher Scientific) in PBS. Cells were blocked for 1 h in 2 % bovine serum albumin (BSA) (Thermo Fisher Scientific) in PBS, stained for 1.5 h with primary and for 1 h with species-matched secondary antibodies at RT and mounted on microscopy slides (Thermo Fisher Scientific) in Fluoromount-G (Sigma-Aldrich) containing DAPI (1:3,000) (Thermo Fisher Scientific). Samples were first stained with biotinylated *Dolichos biflorus* agglutinin (DBA) 1:1,000 (Sigma-Aldrich) and primary monoclonal antibodies (mAb) (anti-rat CC2 1:1,000[45]; anti-mouse myosin heavy chain (MF20) 1:400 (eBioscience™); anti-mouse surface antigen 1 (SAG1) mab DG52 1:500 [46] and then with goat anti-rat-Alexa546 1:300 (Invitrogen), goat anti-rat-Alexa375 1:300 (Thermo Fisher Scientific), rabbit anti-mouse-Cy3 1:400 (Dianova), donkey anti-mouse-Cy5 1:300 (Dianova) or streptavidin-Alexa488 1:2,500 (Invitrogen), and streptavidin-Cy5 1:2,500 (Jackson antibodies). Mitochondrial staining was done prior to fixation for 30 min with Mitotracker™ Deep Red FM (Thermo Fisher Scientific) at 200 nM in tachyzoite medium at 37 °C in a humidified CO_2 incubator. Cultures were chased for 15 min in tachyzoite medium and washed three times with PBS, fixed with 4 % paraformaldehyde followed by immunofluorescence staining as indicated. Monochromatic images were recorded on a Zeiss Apotome Imager equipped with a Plan-Fluar" 63x/1.45 oil M27 objective or on a Zeiss Axio Observer imager equipped with Plan-NeoFluar" 10x/0.3 or a Plan-Apochromat" 63x/1.4 oil objective and imported into ImageJ [47] for coloring and the generation of overlays.

Pepsin digestion and *in vitro* oral transmission assay

KD3 myotube cultures in 6-well plates were infected with $6x10^4$ extracellular Pru-tdTomato tachyzoites corresponding to an MOI of 0.1 and bradyzoite formation was induced for the indicated times in bradyzoite medium. Tachyzoite controls were infected for two days with $3.2x10^6$ parasites corresponding to an MOI of 5 in tachyzoite medium. On the day of experiment, pepsin digestion was performed for 20, 40 and 60 min at 37 °C as described previously [48] using a modified pepsin solution. The buffered solution consisted of 1.01 g pepsin (Thermo Fisher

Scientific), 0.166 g glycine (Thermo Fisher Scientific), 0.129 g NaCl (Sigma-Aldrich) and 17.8 ml of a 1 M HCl solution (Sigma-Aldrich), filled up to 200 ml with Milli-Q-water, resulting in a pH of 1.2 and supplemented with 5 mM glucose. Digestion was terminated by neutralization using a 1.2 % sodium bicarbonate solution (pH≈8.3) containing 0.0159 g/l phenol red as pH indicator dye. Digested infected monolayers and uninfected and undigested controls were collected with a cell scraper and harvested via centrifugation (1,200 x *g*, 10 min). The supernatant was then removed, the pellets were resuspended in 450 µl DMEM tachyzoite medium and used to infect HFF cells in a 96-well plate in triplicates, if not indicated differently. Parasite recovery was monitored by measuring tdTomato fluorescence intensity (excitation 554 nm / emission 589 nm) in a plate reader (Tecan Infinite M200 PRO) every second day for up to 21 days. Medium was carefully exchanged without perturbating infected monolayers after each measurement.

For the oral transmission assay, scraped monolayers and controls were challenged by the indicated combination of stresses: cold stress (4 °C for four and seven days), heat stress (55 °C or 65 °C for 5 min), incubation at RT for two days, and pepsin digestion (60 min).

The resistance score (RS) was calculated as the difference of days passed between the detection of vehicle-treated and treated tachyzoite cultures. This difference was normalized to the number of days of total observation to account for differences in initial cyst loads and the resulting re-growth periods between experiments:

$$RS = 1 - (\#days_{treatment} - \#days_{vehicle}) / \#days_{observed}$$

An RS of 0 indicates no recovery from the treatment and a RS of 1 means equal growth to the vehicle-treated control, indicating full resistance to the treatment.

In vivo **oral transmission assay**

KD3 myotube cultures in 6-well plates were infected with 1.9×10^5 Pru-tdTomato tachyzoites corresponding to a MOI of 0.3. Bradyzoite formation was induced for indicated time in bradyzoite medium. Tachyzoite cultures were prepared in T25 cell culture flasks by infecting KD3 myotubes and human fibroblasts with 3.6×10^6 tachyzoites corresponding to an MOI of 2 for two days in tachyzoite medium. The cultures were then prepared for shipping and sent to Freiburg at RT within 24 h. The cultures were washed once with PBS, scraped in fresh respective medium and harvested via centrifugation (1,200 x *g*, 10 min). The supernatant was removed after centrifugation and the pellet was resuspended in 2 ml PBS and placed on ice. For tachyzoite

controls, scraped monolayers were syringed with a 27G needle (Sterican®) to release intracellular parasites and counted in a Neubauer chamber (Roth). For cyst quantification, 10 µl of the cyst solution was placed on a glass slide and cysts were counted based on the fluorescence of tdTomato in a fluorescence microscope. For *in vivo* cyst generation, one C57BL/6JRj mouse was infected with $1x10^3$ *T. gondii* tachyzoites via intraperitoneal injection. 30 days post infection, the mouse was euthanized by cervical dislocation. The brain was harvested in 2 ml PBS and minced using an 18G and 21G needle (Sterican®) for cysts inspection via DBA staining as described previously[49]. Briefly, 50 µl out of 200 µl DBA-stained sample were pipetted in a clear-bottomed 96 well plate and quantified at 20x magnification using DBA positivity as a first criterion and tdTomato positivity to confirm brain cyst.

Mouse infections

Groups of five 10-week-old male and female mice (C57BL/6JRj) were obtained from certified breeders (Janvier Labs, Route du Genest, 53940 Le Genest-Saint-Isle, France) and kept under specific-pathogen-free conditions in the local animal facility (Department for Microbiology and Hygiene, Freiburg). All animal experiments were performed in accordance with the guidelines of the German animal protection law and the Federation for Laboratory Animal Science Associations. Experiments were approved by the state of Baden-Württemberg (Regierungspräsidium Freiburg; reference number 35-9185.81/G-19/89).

Mice were infected by oral gavage with 50 or 500 freshly prepared *in vitro*-generated Pru-tdTomato cysts, 10 freshly prepared *in vivo*-derived Pru-tdTomato cysts or 10^4 myotube- or HFF-derived extracellular Pru-tdTomato tachyzoites in a total volume of 200 µl sterile PBS.

Infected mice were monitored and weighed daily for the duration of the experiment. Relative weight loss was calculated based on the weight at the day of infection. Brains and blood from moribund animals were collected starting from 12 days post infection. After 30 days post infection, blood samples of all surviving mice were collected from the facial vein. Blood was allowed to clot at RT for 30 min before centrifugation (500 x *g*, 10 min). Serum was collected and either immediately analyzed or stored at -20 °C until further analysis. Animals were euthanized by cervical dislocation. Brains were harvested and cysts per brain sample were blindly counted as described previously:

Cysts/brain = cysts in 50 µl * 40

Seroconversion was evaluated via ELISA as described previously[49]. Serum from non-infected (n.i.) mice were included to calculate the cutoff:

cut-off = mean Absorbance$^{450\ nm-570\ nm}$ (n.i.) + 2 x standard deviation of Absorbance$^{450\ nm-570\ nm}$ (n.i.)

An individual cut-off was calculated per each individual ELISA. In order to compare the *T. gondii* specific-antibody titers from different independent experiments a reactivity index was calculated per sample:

Reactivity index = mean Absorbance$^{450\ nm-570\ nm}$/cut-off.

Reactivity index values higher than one were considered as positive.

Cyst isolation

Uninfected and infected myotubes were prepared. In both cases, two T150 dishes were pooled into one sample. For bradyzoite samples, myotubes were infected with $3.2*10^6$ Pru-tdTomato tachyzoites corresponding to a MOI of 0.3 and cyst formation was induced for indicated time. On the day of harvest, infected samples and uninfected host cell controls were placed on ice, medium was removed and monolayers were washed three times with ice-cold PBS. Cells were then harvested by scraping into 10 ml ice-cold 0.05 % BSA in PBS per T150 dish. Cysts were released from the monolayer via forcing through a 23G needle (Sterican®) 25 times with a syringe and collected via centrifugation (1,200 x *g*, 10 min, 0 °C). The supernatant was removed, the pellet was resuspended carefully in ice-cold 2 % BSA in PBS containing 200 µl DBA-coupled beads (preparation described below) and samples were incubated for 1 h at 4 °C with gentle shaking. Subsequently, the samples were placed in a magnetic stand on ice, washed five times with 0.1 % BSA in PBS to remove cell debris, followed by two washing steps with PBS to remove residual BSA. Cysts and beads were then collected via centrifugation (1,200 x *g*, 10 min, 0 °C), shock frozen in liquid nitrogen and stored at -80 °C until extraction. Tachyzoite samples were generated in T150 dishes by infecting myotubes and HFF cells with $3.2*10^7$ tachyzoites corresponding to an MOI of 3 for 48 h. Medium was replaced by ice-cold PBS and monolayers were scraped and passaged through a 27G needle. Tachyzoites were filter-purified through a 3 µm filter (Whatman) and PBS-washed by centrifugation (1,200 x *g*, 10 min, 0 °C) three times. All samples were extracted simultaneously in 80 % acetonitrile for LC/MS analysis as described below. Bead-only controls were processed equally. Bead-supplemented tachyzoite controls were processed equally

to cyst samples, replacing washing steps via magnetic stand by centrifugation (1,200 x *g*, 10 min, 0 °C).

Preparation of beads

Coupling of Dynabeads™ MyONE™ Streptavdin T1 (Thermo Fisher Scientific) to DBA was done as described in the manufacturer's protocol. Briefly, 200 µl beads/sample were resuspended in 1 ml PBS by vortexing, washed three times with PBS in a magnetic stand and resuspended in 1 ml PBS containing 50 µg DBA / sample. The tube containing the DBA-magnetic bead mixture was incubated on a rotary mixer for 45 min at RT. Uncoupled DBA was removed by washing the coated beads three times with PBS. After washing, the DBA-coated beads were resuspended in 2 ml PBS containing 2 % BSA.

Untargeted metabolic analysis of *in vitro* cysts

For metabolome measurements of tissue cysts and tachyzoites, tachyzoite isolation, cyst maturation and isolation were performed as described above. Metabolites were extracted in 80 % acetonitrile (Carl Roth) and 20 % water (Carl Roth) containing internal standards (phenolphthalein, CAPS, PIPES (Sigma-Aldrich)). Cell pellets were sonicated for 5 min and after centrifugation (21,500 x *g*, 5 min, 0 °C), the supernatants were transferred to MS vials for immediate LC/MS analysis. 5 µl of each sample were collected to generate a pooled biological quality control (PBQC). 20 µl of the *in vitro* cysts, bead control and host cell background samples, and 5 µl of the tachyzoite samples were injected. The injection order of the samples was randomized, blanks and PBQCs were injected periodically. The samples were analyzed on a Q-Exactive Plus mass spectrometer (Thermo Fisher Scientific) via 70k MS1 scans, with intermittent 35k data-dependent 35k MS2 scans in positive and negative mode separately.

Chromatographic separation was achieved on a Vanquish Flex fitted with an ACQUITY UPLC BEH Amide column (Waters). Running a 25 min linear gradient starting with 90 % eluent A (10 mM ammonium carbonate in acetonitrile)/10 % eluent B (10 mM ammonium carbonate in water) and ending with 40 % eluent A/60 % eluent B, followed by washing and equilibration steps.

Compound Discoverer 3.1 software (Thermo Fisher Scientific) was used for peak detection, combination of adducts and compound annotation. Metabolite identifications were based on either retention time and accurate mass match to an in-house library of 160 authentic standards, or by matching accurate mass and MS2 fragments to m/z cloud database (Thermo Fisher Scientific).

Data were exported to Excel for grouping, combination of datasets from positive and negative ionization runs and blank subtraction. Compounds with a coverage less than 50 % in at least one sample group were excluded. All missing values were gap filled with either the respective mean of each sample group or the global minimum intensity when undetected in a sample group. After normalization to the internal standard, the fractional abundances for each sample were calculated and centered between 1 and -1.

Raw data, data curation steps and performed statistics are accessible in table S1 and table S2.

Drug tolerance assays

Myotubes in 96-well plates were infected with $2.4x10^3$ *T. gondii* Pru-tdTomato tachyzoites corresponding to a MOI of 0.1 and cyst formation was induced for indicated times in bradyzoite medium at ambient CO_2 levels, followed by a drug pulse of seven days with respective vehicle as solvent control. Tachyzoite controls were infected with $2.4x10^4$ Pru-tdTomato tachyzoites corresponding to a MOI of 1 in tachyzoite medium for 2 h before the seven-day drug pulse was applied in tachyzoite medium. Parasite recovery was monitored by measuring tdTomato fluorescence for 28 days as described above. Medium was exchanged after each measurement. The resistance score was calculated as described above for pepsin digestion and the oral transmission assay.

(i) Developing drug tolerance. Cysts were generated for indicated times and treated with established antiparasitics (pyrimethamine, sulfadiazine (Sigma)) and 1-hydroxy-2-dodecyl-4(1)-quinolon (HDQ) (a kind gift of Wolfgang Bohne), two bumped kinase inhibitors (BKI1294, BKI1553) [50,51] or 0.2 % DMSO (Thermo Fisher Scientific) as solvent control at the indicated concentrations for seven days. Respective tachyzoite controls were generated by infecting KD3 myotubes for 2 h with $2.4x10^4$ tachyzoites corresponding to a MOI of 1 in tachyzoite medium before treatment.

(ii) Drug resistance of matured cysts vs. tachyzoites. Cyst formation was induced for indicated time and pulsed for seven days with indicated concentrations of sodium fluoroacetate (abcr GmbH) or 0.5 % H_2O as solvent control. Respective tachyzoite controls were generated as described above.

(iii) IC_{50} assay tachyzoites. Growth of tachyzoite controls treated with the indicated concentrations of sodium fluoroacetate was monitored throughout the seven-day drug pulse. The

295 half inhibitory concentration (IC_{50}) values were determined at day seven by fitting the dose-
296 response curve by non-linear regression in GraphPad Prism v8.
297
298 **Statistical analysis**
299 All tests, except statistics of metabolite abundances, were performed in GraphPad Prism v8 as
300 detailed in the results section. Statistical significance of metabolite changes was calculated in
301 Microsoft Excel. Principal component analyses were computed using ClustVis[52].
302

Results

KD3 human myoblasts differentiate into multinucleated myotubes

T. gondii persists in skeletal muscle tissue[53], but robust *in vitro* culture systems supporting long-term maturation of tissue cysts in these natural host cells are lacking. We tested an immortalized human skeletal muscle cell isolate (KD3)[35] for its ability to support the culture of *T. gondii* tissue cysts. Sub-confluent myoblast cultures were differentiated into myotubes through serum starvation for five days until cells fused to multinucleated tubes that were expressing myosin heavy chain (Figure 1A) and developed spontaneous contraction activity (Video S1)[35]. Accordingly, the myogenic index, which reflects the fraction of nuclei residing in cells containing three or more nuclei, rose to 0.3 (Figure 1B).

KD3 human myotubes support development of matured tissue cysts of several *T. gondii* strains

Next, KD3 myotubes were tested for their ability to support long-term maturation of *T. gondii* cysts. We infected myotubes with Pru-tdTomato parasites, a type II Prugniaud strain constitutively expressing the tandem (td) Tomato variant of the red fluorescent protein, for up to 21 days. Evaluation of the ultrastructure of the encysted parasites by electron microscopy (Figure 2A, S1) revealed hallmarks of bradyzoites including abundant amylopectin granules to posteriorly positioned nuclei after seven days of infection. The formation of the cyst wall is indicated by the apparent deposition of electron-dense vesicular-tubular material along the parasitophorous vacuolar membrane throughout the course of infection (Figure S1D)[54].

T. gondii strains differ greatly in their capacity to form tissue cysts *in vitro* and *in vivo*[55] and their maturation is accompanied by sequential regulation of marker protein expression[56]. To test the suitability of KD3 myotubes to culture tissue cysts of multiple *T. gondii* strains, we monitored the formation of tissue cysts of eight parasite strains of three major isotypes under CO_2-deplete conditions at neutral and basic pH. Stage conversion was detected by staining the cyst wall with *Dolichos biflorus* agglutinin (DBA) and antibodies against the CC2 protein[45] and by the absence of the tachyzoite-specific surface antigen 1 (SAG1) (Figure 2B). Myotubes infected with type I RH-*Δku80* parasites that do not easily form tissue cysts *in vitro* served as a tachyzoite control.

Strikingly, under both conditions all observed vacuoles of every tested strain were DBA-positive and remained stable without being overgrown by tachyzoites for 21 days. This was also true for the hard to differentiate RHΔ*ku80* (Figure S2). We observed almost complete differentiation of

type III VEG parasites into DBA- and CC2-positive and SAG1-negative cysts. All type II strains and the type III NED strain showed intermediate maturation (between 35 % and 63 %) that was considerably increased in basic pH to 73 % and 83 %, respectively. Also, wild-type type I strains GT1 and RH exhibited differentiation up to 30 % that increased to 77 % and 55 % at basic pH, respectively. As expected, the high-passage laboratory strain RH*Δku80* did not lose SAG1 signal at neutral pH but required basic conditions (Figure 2C).

To directly relate the capability of KD3 myotubes to generate mature bradyzoites to existing culture methods, we differentiated Pru-tdTomato parasites for up to 21 days in HFF, KD3 myoblasts and KD3 myotubes by bicarbonate starvation at pH 7.4 (Figure S3A) and pH 8.3 (Figure S3B). In both conditions, parasites in myoblasts and HFF cells lysed host cells after 14 and 21 days respectively. Only in myotubes, Pru-tdTomato parasites formed an increasing fraction of DBA-positive and SAG1-negative cysts, while SAG1-positive and DBA-negative tachyzoites remained undetectable.

We also tested spontaneous stage conversion under standard bicarbonate-replete conditions as observed in the murine skeletal muscle cell line C2C12[57]. To this end, we infected myoblasts, myotubes and HFF cells with Pru-GFP parasites which express GFP through the bradyzoite-specific LDH2 promoter[40] for 96 h (Figure S4). GFP-negative tachyzoites continued to proliferate in HFF cells and myoblasts leading to host cell lysis. In contrast, proliferation of *T. gondii* appeared attenuated and spontaneous formation was indicated by DBA staining and GFP expression (Figure S4).

Together, these data show that KD3 myotubes enable the culture of tissue cysts of multiple parasite strains at physiological pH over the course of 21 days and augment spontaneous stage conversion.

KD3 myotubes-derived tissue cysts harbor pepsin- and temperature stress-resistant bradyzoites

To test whether *in vitro* bradyzoites also develop functional hallmarks of *in vivo* bradyzoites, such as resistance to temperature stress and pepsin digestion[33], we infected myotubes with Pru-tdTomato parasites and then differentiated parasites for up to 35 days (Figure 3A). Intracellular cysts were digested with pepsin for 20, 40 and 60 min, the reaction mix was then neutralized and cysts were seeded onto HFF cells to allow re-differentiation in tachyzoite medium under CO_2-replete conditions. Untreated and pepsin-digested tachyzoite cultures served as positive and

365 negative controls, respectively. Growth of both, untreated tachyzoite and bradyzoite cultures, was
366 observed by an increase in red fluorescence (indicative of tachyzoite replication) after two and
367 seven days, respectively (Figure 3B). Interestingly, all pepsin-treated bradyzoite cultures
368 recovered after 7, 9 and 14 days, depending on the length of the pepsin digest, while pepsin-
369 digested tachyzoite cultures did not recover even after a period of 21 days. We quantified pepsin
370 resistance across the time course of cyst maturation by calculating a resistance score (RS) (see
371 Material and Methods) based on the pepsin-inflicted growth delay (Figure 3C). Already after 14
372 days all digested cultures recovered with an RS between 0.4 to 0.5. Pepsin resistance continued
373 to increase over the course of 28 days up to an RS of 0.8 (Figure 3C).

374 In human transmission scenarios, encysted bradyzoites survive extended cold-storage and heat
375 stress[33]. To test whether *in vitro* bradyzoites would survive under these conditions, cysts were
376 matured for 35 days and treated with a combination of (1) storage as cell 'pellets' at 4 °C for up
377 to seven days, (2) a 5 min heat shock at 55 °C or 65 °C and (3) pepsin digestion for 60 min (Figure
378 3D). Storage at room temperature (RT) for two days served as a positive control and did not
379 decrease viability in comparison with untreated cysts, as indicated by an RS of 1. Different
380 combinations of storage at 4 °C for four or seven days and heat shock at 55 °C did lower the RS
381 to a range between 0.75 and 0.65, while heating to 65 °C effectively killed tissue cysts as
382 expected[33]. These results demonstrate that myotube-grown encysted bradyzoites develop traits
383 that are important for oral transmission of tissue cysts as it occurs with cysts in muscle tissues of
384 farm animals.

385 Summarized, these data indicate that KD3 myotubes support maturation of *T. gondii* tissue cysts
386 for 35 days. These *in vitro* bradyzoites develop of resistance to pepsin and temperature stresses,
387 which are functional hallmarks of mature *in vivo* bradyzoites and required properties for both
388 experimental oral infection of mice and environmental transmission to humans.

389 **KD3 myotube-derived tissue cysts are orally infectious to mice**

390 To assure oral infectivity to animals, groups of five mice were infected with 50 and 500 35-day-
391 old *in vitro* cysts via oral gavage. Control groups included mice receiving 10^4 fibroblast- or
392 myotube-derived tachyzoites and as positive control 10 *in vivo* tissue cysts prepared 35 days post
393 infection from brain tissue. To facilitate the comparison of infectivity between *in vitro* and *in vivo*
394 cysts, we estimated relative volumes of *in vitro* cysts by measuring their diameters (Figure 4A).
395 Maturation over the course of 35 days increased the average diameter from 8.8 µm to 11 µm.
396 This compares to 35-day-old *in vivo* cysts from brain tissue with a mean diameter of 56 µm [22].

Assuming spherical cysts, this implies an approximate 150-fold difference in volume. Infection of mice with 50 and 500 *in vitro*-derived cysts led to seroconversion of 8 out of 10 and 9 out of 10 mice, respectively (Figure 4B, D). We also observed seroconversion of 1 and 2 mice infected with HFF- and myotube-derived tachyzoites. As expected, all mice infected with 10 *in vivo*-derived tissue cysts showed seroconversion. Infection was also indicated by weight loss of mice receiving 500 *in vitro* or 10 *in vivo* cysts. In these groups two animals succumbed to the infections while one animal that received 50 cysts needed to be culled (Figure S6A, B). The presence of DBA-positive *T. gondii* cysts in the brains of infected mice was quantified microscopically 30 days post infection in brain homogenates (Figure 4 C, D). We detected cysts in all seroconverted tachyzoite infected mice and mice receiving 500 *in vitro* cysts or 10 *in vivo* cysts. Only one of three mice that seroconverted from infection with 50 cysts and survived, harbored detectable cysts.

Together these data indicate that KD3 myotube derived tissue cysts develop oral infectivity to mice that is similar to *in vivo* cysts.

KD3 myotube-derived tissue cysts develop resistance against antiparasitics.

T. gondii tissue cysts largely resist current toxoplasmosis treatments. To test whether cysts cultured in myotubes mirror drug resistance *in vivo*, we exposed 14-, 21- and 28-day-old Pru-tdTomato-expressing cysts to antiparasitics for seven days and monitored their re-differentiation into tachyzoites under CO_2-replete conditions as a measure of bradyzoite viability (Figure 5A). Figure 5B shows the fluorescence signal observed over 49 days, including 14 days of cyst maturation, seven days of pyrimethamine treatment, and 28 days of re-differentiation. Growth of DMSO- and pyrimethamine-treated parasites was indicated by an increase in fluorescence above background at 14- and 24-days post treatment, respectively (Figure 5B). Next, 14-, 21- and 28-day-old tissue cysts were treated with 5 µM and 20 µM pyrimethamine, 20 µM sulfadiazine and 0.1 µM of 1-hydroxy-2-dodecyl-4(1)-quinolon (HDQ), an inhibitor of dihydroorotate dehydrogenase (DHOD)[58] and alternative NADH dehydrogenase[59] (Figure 5C). Bradyzoite cultures survived all tested treatments. Interestingly, while resistance against sulfadiazine, HDQ or low doses of pyrimethamine was already fully developed after 21 days, indicated by an RS of 1, resistance against high doses of pyrimethamine increased until 28 days of maturation (Figure 5C). In contrast, tachyzoite-infected myotubes, which served as a control and are shown as ‘0 days differentiated cultures’, only marginally survived treatment with 5 µM pyrimethamine, with a low RS of 0.18. While resistance of bradyzoites to antifolates is well established resistance to mitochondrial inhibitors is less well documented. We sought to test

whether exclusion of HDQ by the cyst wall would lead to insensitivity and thus monitored resistance and mitochondrial membrane potential of 28-day old cysts. Up to one 1 µM of HDQ did not decrease the RS and cyst diameter but decreased the mitochondrial membrane potential estimated by the drop of intensity of Mitotracker staining intensity by 60 % (Figure SA-D). Furthermore, we tested the resistance against two different bumped kinase inhibitors (BKI), BKI1553 and BKI1294 (Figure 5D), that have been shown to decrease cyst burden in chronically infected mice[60,61]. Consistent with previous results, tachyzoites did not grow after exposure to fourfold of the IC_{50} of each compound. In contrast, already 14-day-old tissue cysts were resistant to both treatments, with an RS of 0.42 and 0.83, respectively. Resistance increased further and BKI1553 became completely ineffective against 28-day-old cysts while cysts reached an RS of 0.89 against BKI1294 (Figure 5D).

Taken together, these data demonstrate that myotube-cultured cysts gradually develop resistance against both established and experimental antiparasitics and are suited for compound screens against chronically infectious forms of *T. gondii*.

The metabolome of *T. gondii* depends on the host cell type and parasite stage

The metabolome is directly linked to the mode of action of many antiparasitics and may also be associated with their efficacy [5]. However, the metabolome of bradyzoites and its differences to tachyzoites remains largely unknown. To test whether bradyzoites possess a distinct metabolome, we compared the abundance of metabolites between ME49 parasites in their bradyzoite form with intracellular tachyzoites in both HFF cells and myotubes (Figure 6). Parasites were differentiated into cysts for 28 days, quenched with ice-cold PBS, released from cells by needle passage and purified from host cell debris via binding to DBA-coated magnetic beads. We estimated a yield of $2x10^6$ cysts from two pooled T150 culture dishes that were used for one replicate (data not shown). Intracellular tachyzoites were prepared by needle passage and filtered to remove host material. We also estimated artefacts that are introduced by differences in quenching and preparation procedures of tachyzoites and bradyzoites. We supplemented isolated tachyzoites with beads and processed them similarly to bradyzoites. To correct for background metabolites from contaminating host material and magnetic bead preparations, we included uninfected myotubes and bead-only controls into our analysis. These samples were treated identically to bradyzoite samples. All preparations were extracted in 80 % acetonitrile and analyzed on a HILIC-UHPLC-LC/MS. Blank and host cell background subtracted ion intensities were normalized to the total ion count per sample and log2-fold changes of metabolites between experimental conditions calculated (Figure S8A-F, Table S1).

Principal component (PC) analysis indicated that bradyzoites in the purified tissue cysts differed from tachyzoites along PC1, while myotube- and HFF-derived tachyzoites were separated in PC2 (Figure 6A). Bead-supplemented tachyzoite controls that underwent incubation with similar purification procedure as tissue cysts and were incubated with beads for one hour were indistinguishable from pure tachyzoites.Uninfected host cells controls were similar to bead-only samples, indicating minimal metabolite alterations and contamination due to the purification procedures (Figure S8E). The two clusters of HFF-derived tachyzoites represent two independent experiments whose variation manifests itself after host-background subtraction (Figure S8D). We quantified the levels of 71 metabolites, excluding those that we detected in uninfected controls. The levels of 26 metabolites varied between parasite stages, 10 varied between types of host cells, while 24 depended on both factors, and 11 remained invariant (Figure 6B-D). Comparing bradyzoites to tachyzoites from the same host cell type (Figure 6E), we noted that the relative abundances of amino acids and sugar derivatives were generally increased, while vitamins, derivatives of amino acids, nucleic acids and metabolites associated with the tricarboxylic acid (TCA) cycle were significantly decreased. Fatty acids (FAs) and related molecules are variably affected by stage conversion. When comparing tachyzoites from HFF cells with those from myotubes (Figure 6E), we found that the levels of amino acids and sugars were higher in HFF-grown tachyzoites, while FAs increased in abundance. The host cell type had mixed effects on other metabolite classes.

These data reveal distinct metabolic features in *T. gondii* bradyzoites involving various metabolite classes and the mitochondrial TCA cycle.

Mature *T. gondii* tissue cysts develop resistance against the aconitase inhibitor sodium fluoroacetate

We hypothesized that diminished pools of TCA metabolites in bradyzoites would be consistent with lower importance in this stage. To estimate the reliance of bradyzoites on the TCA cycle, we used the aconitase inhibitor NaFAc to inhibit the TCA cycle flux in *T. gondii* [6]. Continuous exposure to NaFAc arrests tachyzoite replication with an IC_{50} of 168 µM, and parasite replication was minimal at 500 µM (Figure 7A). Next, we tested the ability of tachyzoites and bradyzoites to survive exposure to 0.5 to 5.0 mM NaFAc for seven days. 28-day-old cysts recovered after treatment with a RS of approximately 0.8, while tachyzoites were only able to survive 0.5 mM NaFAc, but not higher concentrations (Figure 7B). To exclude that tolerance of bradyzoites towards NaFAc relies on exclusion of this inhibitor from the cyst wall [62], we sought to measure marked direct metabolic effects of this inhibitor on tachyzoite and bradyzoite

stages[6]. We treated 28-day-old ME49 cysts and intracellular myotube-cultured tachyzoites with NaFAc for seven and three days, respectively and analyzed the metabolomes by HILIC-UHPLC-LC/MS (Figure 7C-D, Table S2). The PC analysis revealed that solvent- and NaFAc-treated tachyzoites form distinct clusters that are separated along the PC2 axis. In contrast, treatment of tissue cysts did not lead to a separation from untreated controls (Figure 7C). NaFAc treatment affected the relative abundance of 33 metabolites in tachyzoites, but changed only 8 metabolites in bradyzoites (Figure 7D). Aconitate levels in both parasite stages were increased significantly upon NaFAc treatment (Figure 7D).These data are consistent with a NaFAc-mediated inhibition of aconitase in bradyzoites and show that extended exposure to high doses of this inhibitor, in contrast to tachyzoites, is well tolerated.

Discussion

Persistence mechanisms of important protozoan pathogens, including *T. gondii*, *T. cruzi*, *Leishmania* spp. and *P. vivax,* remain largely understudied, and there are inadequate or no treatments available against chronic infections with these organisms[2]. The limited availability of methods to culture persister cells restricts the approaches to study the link between persistence and metabolism[2,63]. Here, we report a cell culture model based on immortalized human skeletal muscle cells[35] that supports maturation of tissue cysts of type I, II and III *T. gondii* strains. These myotube-grown bradyzoites exhibit key characteristics including typical ultrastructural features, stress resistance and tolerance towards antimicrobials.

Our *in vitro* system is scalable, enabling measurements of bradyzoite metabolites via mass spectrometry. To this end, we established a protocol that allows isolation and purification of cysts in large quantities and without the use of Percoll gradients[22], making them available for mass spectrometry-based metabolomics. We obtained an estimated yield of $2x10^6$ cysts per two T150 culture dishes that were sufficient for one technical replicate and represented a volume-adjusted 10-fold improvement to the bradyzoite yield form the infection of one mouse [22]. Principal component analysis of the impact of host cell type and the parasite stage indicates mostly independent effects on the metabolome (Figure 5A). Stage conversion leads to changes that are largely homogeneous across classes of metabolites such as amino acids, vitamins, TCA cycle intermediates and nucleic acids. This indicates the operation of distinct metabolic homeostasis mechanisms in bradyzoites.

Bradyzoites harbor lower levels of several TCA cycle-associated metabolites that are consistent with a lower reliance on this pathway (Figure 6E). This interpretation is supported by an NaFAc-

induced slight accumulation of aconitate (Figure 7B). Extensive accumulation of citric acid and aconitate has previously been shown to occur in extracellular tachyzoites already after four hours of treatment[6]. We attribute the lower accumulation of aconitate we observe in bradyzoites to the extended treatment over seven days and the longer quenching and purification procedure required for intracellular parasites. Importantly, this accumulation of aconitate suggests that NaFAc is available to bradyzoites, that the aconitase is active and inhibited by NaFAc. This interpretation also agrees with previous findings of an active TCA cycle enzyme, isocitrate dehydrogenase, in lysates of four-week-old bradyzoites from mice[64] and with continued transcription of TCA-cycle related genes[65]. Interestingly, NaFAc exerts comparatively limited effects on other non-TCA cycle-related metabolites in bradyzoites. It is noteworthy that our data do not exclude the possibility that parts of the TCA cycle remain operational and may process anaplerotic substrates, such as glutamine to generate NADH for subsequent ATP production through the mitochondrial electron transport chain (mETC). However, full resistance to the inhibitor of the alternative type 2 NADH-dehydrogenase TgNDH2[66] (Figure 5C, Figure S7C-D) suggests that this source of ATP would equally be dispensable. HDQ appears to only partially decrease the mitochondrial membrane potential in bradyzoites (Figure S7A-B), indicating the presence of HDQ-independent sources of reduction equivalents or a very slow rate of mitochondrial ATP synthesis concomitant with negligible depolarization of the membrane potential. Bradyzoites may rely increasingly on glycolytic ATP production, as indicated by increased activity of glycolytic enzymes in this stage[64]. The number of *T. gondii* cysts in brain tissue of latently infected mice depends on the turnover of large amylopectin pools[67] and on the expression of several glycolytic enzymes including hexokinase[11] and lactate dehydrogenase[12,68]. Also, the pyruvate dehydrogenase E1 subunit transcript is less abundant in four-week-old bradyzoites[69]. Interestingly, transcriptomic analyses of *P. vivax* hypnozoites, a persistent stage of this malaria parasite, indicates a similar metabolic shift towards glycolysis[70].

We also found that a number of amino acids were accumulated in bradyzoites (Figure 6E). We attribute these changes directly to stage conversion and not to differences in media composition. The affected amino acids, except for proline, which can also be synthesized from glutamate[71], are less concentrated in the RPMI-based bradyzoite medium compared to the DMEM-based medium used for tachyzoites. All of these amino acids have been shown to be imported by extracellular tachyzoites[72]. *T. gondii* tachyzoites express several Apicomplexan Amino Acid Transporters (ApiATs)[72], all of which remain transcriptionally expressed in bradyzoites[69] (Figure S9). This suggests that bradyzoites retain the ability to take up amino acids from their environment.

Interestingly, restriction of some exogenous amino acids has been used to facilitate stage conversion[63,73] suggesting that alternative sources may represent adaptions to limiting supply of exogenous amino acids. These include obligate autophagy and proteolysis through autophagy-related protein (ATG9)[19] and cathepsin L[74] and lower amino acid demand by translational repression through the eukaryotic initiation factor 2α[75]. The diversification of nutrient sources would resemble the stringent metabolic response of *Leishmania mexicana* amastigotes that also adopt a slow growing phenotype within the phagolysosome of macrophages[76].

Nucleobase-containing metabolites were found to be less abundant in bradyzoites (Figure 6E). While the parasite is auxotroph for purines, pyrimidines can both be imported and synthesized[77]. Slowly growing or dormant bradyzoites likely require lower amounts of nucleobases. Consistently, the transcription of the corresponding low affinity and high-capacity adenosine transporter TgAT[78,79] appears to be down-regulated in 4-week-old bradyzoites *in vivo* (Figure S9). Two other proteins containing nucleoside transport signatures remain expressed and may represent the unidentified high-affinity purine transporter being responsible for maintaining a slow influx of nucleobases[69] (Figure S9). Pyrimidine salvage does not appear to be essential for bradyzoite formation[80] indicated by its continued synthesis. Similar to *P. falciparum*[81], pyrimidine synthesis in *T. gondii* tachyzoites depends on the mitochondrial electron transport chain (mETC) to provide an electron acceptor to the dihydroorotate dehydrogenase (DHOD)[82]. The role and relevance of the mETC in bradyzoites remains to be formally established. While we show that *in vitro* bradyzoites develop tolerance towards the dual alternative NADH dehydrogenase and DHOD inhibitor HDQ[58,83] (Figure S7D), other mETC inhibitors, such as atovaquone appear to have some effect and lead to a decrease in cyst counts in brains of latently infected mice[15-17,84]. Activity of atovaquone against *in vitro* tissue cysts could not be conclusively assessed due to the lack of a treatment window in KD3 myotubes (data not shown). Together, available data suggests that the mETC is a viable target in tissue cysts but that the importance of the associated metabolic pathways, such as the TCA cycle may differ from tachyzoites.

Multinucleated myotubes are generally arrested in the G0 phase of the cell cycle and exhibit highly branched mitochondria and oxidative metabolism as opposed to glycolytic lactate production[85]. Both traits have been shown to also facilitate stage conversion of *T. gondii*[27,86,87] and may contribute to the suitability of KD3 cells to harbor *T. gondii* tissue cysts by limiting the expansion of non-converting tachyzoites. While the differentiation efficiency of all tested *T. gondii* strains can

592 be further increased by additional non-physiological stressors such as basic pH, it is not needed
593 for extended cultures. Strikingly, even highly virulent RH-derived parasite sub-strains did not
594 overgrow the culture (Figure 2C). Resistance of bradyzoites against pepsin digestion and
595 temperature stress develops after 14 days post infection and increases until 28 days post infection
596 (Figure 3C). The onset of tolerance towards inhibitors of well-established drug targets including
597 the calcium-dependent protein kinase 1 (TgCDPK1)[60,61], dihydrofolate reductase-thymidylate
598 synthase (TgDHFR-TS)[88] and the DHOD (Figure 5C-D) follows similar timing and is shared with
599 *T. gondii* cysts in the brain of chronically infected mice[59-61,89]. Hence, our *in vitro* model will
600 facilitate dissecting the molecular basis of the impressive drug tolerance and stress resistance of
601 *T. gondii* tissue cysts. Expectedly, *in vitro* cysts are also orally infectious to mice (Figure 4A-D).
602 Comparing estimated volumes of *in vitro* cysts and *in vivo* brain-derived cysts, our data suggest
603 that 10 *in vivo* cysts are equivalent to 500 *in vitro* cysts in this regard. Surprisingly, 3 out of 20
604 mice that received tachyzoite via oral gavage seroconverted. This has been observed earlier were
605 numbers greater than <1000 pepsin-sensitive tachyzoites were orally infectious to mice[48].

606 Electron microscopic analysis of the ultrastructure of myotube-derived tissue cysts revealed
607 typical features such as a developing cyst wall, amylopectin granules and posteriorly positioned
608 nuclei in the bradyzoites (Figure 2A, S1)[90]. Interestingly, we also found evidence of disintegrating
609 bradyzoites at all time points up to 21 days post infection, (Fig S1) that has also been described
610 previously in mice after four and eight weeks of infection[22,90,91]. This parasite turnover likely
611 contributes to the heterogeneous appearance with respect to cyst size and bradyzoite packaging
612 density[21,22]. A similar phenotypic heterogeneity has been ascribed to the ability of other
613 intracellular pathogens to persist in the presence of stressors such as drugs and immune
614 effectors[92].

615 In conclusion, we present a novel system to culture functionally mature *T. gondii* tissue cysts that
616 surpasses typical *in vivo* systems through its scalability. Importantly, it allows cyst purification with
617 methods compatible with subsequent mass spectrometry-based applications. We show that
618 bradyzoites maintain a distinct metabolome and that confers resistance to an aconitase inhibitor
619 . This culture model will be valuable for uncovering new bradyzoite biology and for addressing
620 drug tolerance.

Acknowledgements / Funding

We are grateful to Naohiro Hashimoto for sharing KD3 skeletal muscle cells, David Sibley for sharing DG52 antibodies, Wesley Van Voorhis and Wolfgang Bohne for sharing BKIs and HDQ, respectively; Alexander Neumann for sharing CCEAN software; Gereon Schares, Marie-France Cesbron-Delauw, Jonathan Howard, Boris Striepen and Dominique Soldati-Favre for *T. gondii* strains and Anton Aebischer and Dominique Soldati-Favre for helpful discussions. MB, CC, DM, EH, JS, FM are funded by the Federal Ministry of Education and Research (BMBF) under project number 01KI1715 as part of the "Research Network Zoonotic Infectious Diseases". FS is a senior member of graduate schools GRK 2046 and IRTG 2290, supported by the German Research Council (DFG). TS receives support from the Deutsche Forschungsgemeinschaft (DFG) (STE 2348/2), MML is funded (Research Grants-Doctoral Programs in Germany) by the German Academic Exchange Service (DAAD). MB, CC, DM, EH, JS, FM, TH and FS receive internal support from the Robert Koch-Institute.

Data availability

Authors can confirm that all relevant data are included in the paper and/or its supplementary information files.

Author Contributions

Conceptualization: M.B.; C.C.; Methodology: M.B., F.S., C.C., D.M., M.M.L., T.S.; Investigation: C.C., D.M., E.H., M.M.L., T.H., J.S.; Writing –Original Draft: M.B. and C.C.; Writing –Review & Editing: all authors; Funding Acquisition: M.B.; Supervision: M.B., F.S., T.S.

Declaration of Interests

The authors declare no competing interests.

Main Figures

Figure 1: KD3 human myoblasts form multinucleated myotubes. (A) Immunofluorescence images of KD3 myoblasts and myotubes after five days of differentiation stained for myosin heavy chain (MF20) and DNA (DAPI). Scale bar indicates 100 µm. (B) As a morphological parameter of myotube formation, the myogenic index (number of nuclei residing in cells containing three or more nuclei, divided by the total number of nuclei) was measured in at least 10 different randomly selected locations by CCEAN software[95]. Values are expressed as mean ± SEM of two individual experiments performed in triplicates (***p<0.001, Mann-Whitney-U-test).

Figure 2: Time- and pH-dependent cyst maturation of type I, II and III *T. gondii* strains in KD3 myotubes. (A.) Electron microscopy of 7-, 14- and 21-day-old Pru-tdTomato tissue cysts in KD3 myotubes (days post-infection; d.p.i.). Cysts show a distinct wall (CW) and are densely packed with parasites containing amylopectin granules (A) and nuclei (N). (B) Immunofluorescence imaging of KD3 myotubes infected with type I (RH, RHΔ*ku80*, GT1), type II (ME49, NTE, Pru-tdTomato) and type III (NED, VEG) parasites. Cyst formation was induced for 7, 14 and 21 days under neutral or basic pH and stained with anti-CC2, anti-SAG1 antibodies, DBA and DAPI. Shown are representative images of tachyzoite controls infected with RHΔ*ku80* for 24 h (upper panel), 14-day-old intermediate cysts (middle panel) and mature cysts (lower panel) of the NED strain. Scale bar indicates 5 µm (C.) Relative numbers of SAG1-negative but DBA and CC2-positive cysts counted from three independent blinded experiments performed in triplicates. At least 25 DBA positive cysts per strain, time point and replicate were counted. Values represent means ± SEM.

Figure 3: *In vitro* bradyzoites develop resistance to pepsin and tolerance to temperature stresses. (A.) Experimental design of *in vitro* pepsin and oral transmission assay. Pru-tdTomato cysts and tachyzoite controls were challenged with indicated pepsin and/or temperature stresses. Treated parasites were seeded onto fresh human fibroblasts to induce tachyzoite re-differentiation and proliferation. tdTomato fluorescence was monitored in a fluorescent based plate reader. (B.) Raw fluorescence intensities of 21-day-old cysts digested for 20 (red), 40 (blue) and 60 min (green) and the respective tachyzoite control (grey). Dashed lines indicate corresponding untreated controls. The data represent the means and SEM of one experiment consisting of three digestion reactions (C.) Resistance scores of tachyzoite cultures (0), 14-, 21- and 28-day-old cysts after 20 (red), 40 (blue), 60 min (green) of pepsin digestion. Shown are the means and SEM of three independent experiments performed in triplicates (*p≤0.05, Mann-Whitney-U-test). (D.) Resistance scores of 35-day-old bradyzoites exposed to indicated temperature stresses and pepsin digestion. Values are expressed as means and SEM from three or two independent experiments in triplicates (**p<0.005, ***p<0.001, Mann-Whitney-U-test).

Figure 4: *In vitro* cysts are orally infectious to mice and lead to manifestation of chronic infection. (A.) Quantification of cyst diameter of 7-, 14-, 21, 28 and 35-day-old Pru-tdTomato *in vitro* tissue cysts. Encysted bradyzoites were stained with DBA and DAPI. Images of 50 cysts were randomly recorded and the diameter was measured by defining the DBA stain as the outline of the cysts. Values are expressed as means and SEM from one experiment. (B.-D.) Reactivity index and cyst number per brain of mice that were orally infected with 10^4 HFF- or myotube-derived tachyzoites, 50 or 500 35-day-old Pru-tdTomato *in vitro* cysts or 10 Pru-tdTomato *in vivo* cysts. Brains and blood from moribund animals were collected starting from 12 days post infection. (B.) Seroconversion was checked for *T. gondii* specific IgGs via ELISA and reactivity index was calculated. Values are expressed as means and SEM from two independent experiments consisting of five mice per group. (C.) Quantification of cyst burden in brains of infected mice. Only seropositive mice from one experiment were analyzed for brain cysts. Values are expressed as means and SEM. (D.) Summary of *in vivo infection* experiments. †: infected animals died during the 30-day period. * Seroconversion of moribund, but not dead animals were checked throughout the experiment. ** Brain cyst burden was only determined in seropositive animals of one experiment.

Figure 5: *T. gondii in vitro* bradyzoites develop broad drug tolerance. (A.) Experimental design for *in vitro* drug tolerance assay. Pru-tdTomato cysts and tachyzoite controls were drug treated at the indicated concentrations for one week. Following the treatment, medium was changed to bicarbonate-replete medium to induce re-differentiation to proliferating tachyzoites and tdTomato fluorescence was monitored. (B.) Raw fluorescence intensities of a representative experiment during cyst maturation for 14 days, 7 days of treatment with 20 µM pyrimethamine or 0.2 % DMSO as solvent control and re-differentiation for 28 days. Black dotted line indicates the limit of detection. Data represents the means and SEM of one experiment with five replicates. (C.-D.) Resistance scores of tachyzoites (0) and 14-, 21- and 28-day-old bradyzoites treated with pyrimethamine (PYR), sulfadiazine (SULF) or 1-hydroxy-2-dodecyl-4(1*H*) quinolone (HDQ) and bumped kinase inhibitor (BKI) 1553 and BKI 1294. Shown are means of three independent experiments with five replicates each and SEM (*p≤0.05, Mann-Whitney-U-test).

Figure 6: *T. gondii in vitro* tissue cysts harbor a distinct metabolome (A.) Principal component analysis of untargeted metabolomic data comparing 28-day-old ME49 *T. gondii in vitro* cysts cultivated in KD3 myotubes, tachyzoites in KD3 myotubes (MT) and tachyzoites in human fibroblasts (HFF). Two individual experiments with four replicates each were analyzed. (B.) Pie chart showing the number of metabolites within the dataset and how they were affected by host cell environment and parasite stage. (C.-D.) Volcano plots of log2-fold changes calculated from fractional metabolite abundances between (C.) *in vitro* cysts and myotube-isolated tachyzoites or (D.) tachyzoites isolated from HFFs and myotubes (n=8, Mann-Whitney-U-test). (E.) Heatmap showing log2-fold changes of significantly different metabolites ($p<0.05$, uncorrected Mann-Whitney-U test) between *in vitro* cysts and tachyzoites (Tz) in MTs (left panel) and tachyzoites in HFFs compared to tachyzoites in myotubes (right panel). Log2-fold changes

were calculated pair-wise. Grey areas indicate non-significantly changed metabolites. Asterisks denote putative metabolite identifications based on accurate mass only. Ac: acetyl, UDP-NAc-GlcN: UDP-N-acetyl-glucosamine, GABA: γ-aminobutyric acid, GroPIns: glycerphosphoinositol, GroPEtn: glycerophosphoethanolamine, G3P: glycero-3-phosphate.

Figure 7: Bradyzoites develop resistance to an aconitase inhibitor.. (A.) Calculation of half inhibitory concentration (IC_{50}) of sodium fluoroacetate (NaFAc) for Pru-tdTomato tachyzoites. Parasites were grown for seven days in presence of NaFAc and the IC_{50} value was calculated from fluorescence intensities normalized to untreated controls. Shown are means and SEM of three independent experiments with three replicates each. (B.) Resistance scores of tachyzoites and 28-day-old bradyzoites treated with NaFAc or 0.5 % water as solvent control. Shown are means and SEM of two and three independent experiments for bradyzoites and tachyzoites performed in triplicates, respectively (*p ≤ 0.05, Mann-Whitney-U-test). (C.) Principal component analysis of untargeted metabolomic data comparing 28-day-old ME49 *T. gondii in vitro* cysts cultivated in KD3 myotubes either incubated for 7 days in presence of 1 mM NaFAc or 0.5 % water as solvent control and tachyzoites cultivated in myotubes treated for three days with 500 µM NaFAc or 0.25 % water as solvent control. One experiment with four replicates for bradyzoite groups, five replicates for solvent treated and three replicates for NaFAc treated tachyzoites were analyzed. (D.) Heatmap showing log2-fold changes of significantly different metabolites ($p<0.05$, uncorrected Mann-Whitney-U test) between NaFAc treated and vehicle treated *in vitro* cysts and between NaFAc treated (left panel) and vehicle tachyzoites (Tz) (right panel). Log2-fold changes were calculated pair-wise. Grey areas indicate non-significantly changed metabolites. Ac: acetyl, G3P: glycerol 3-phosphate.

Supplemental Information

Video S1: Spontaneous contraction of differentiated KD3 human myotubes. Short video sequences were recorded on a Zeiss Observer equipped with a 63X oil immersion objective

Figure S1: Micrographs of maturing Pru-tdTomato in KD3 human myotubes. Electron microscopy of (A.) 7-, (B.) 14- and (C.) 21-day-old Pru-tdTomato tissue cysts matured in KD3 myotubes as shown in Figure 2 (p.i.: post infection). Images of a single section plane through entire cysts were taken for each time point. Each overview image (upper left) is grouped with three images showing enlarged areas, such as individual parasites with their nuclei (N), amylopectin granules (A) or the cyst wall (CW). In the example shown here, the cyst wall is already well developed 7 days post infection. Other cysts at this time point reveal an immature cyst wall, which is shown in the left image of the additional image panel on the lower right side (D.). At this stage the parasitophorous vacuolar membrane (PVM) is associated with a loose matrix containing vesicles and membrane-bound tubules. In cysts 21 days post induction (shown at the right side of this image panel), the cyst wall (CW) is formed by a dense and rather homogenous matrix, which is associated with the PVM.

Figure S2: Immunofluorescence imaging of KD3 myotubes infected with type I RHΔ*ku80*. Cyst formation was induced for 7, 14 and 21 days under neutral or basic pH and stained with anti-SAG1 antibodies, DBA and DAPI. Shown are representative images of 21-day-old RHΔ*ku80* tissue cysts cultured in neutral (left image) and cultured in basal pH (right image). Scale bar indicates 50 µm.

Figure S3: Time- and pH-dependent maturation of type II Pru-tdTomato parasites in human fibroblasts, human KD3 myoblasts and myotubes. (A.-B.) Cyst formation was induced for 7, 14 and 21 days in human fibroblasts, KD3 myoblasts and myotubes under neutral (A.) or basic (B.) pH and stained with anti-SAG1 antibodies, DBA and DAPI. Displayed are percentage of vacuoles that only expressed SAG1 but not DBA, vacuoles that co-expressed SAG1 and DBA and vacuoles that exclusively expressed DBA but lacked SAG1. Values represent means from one blinded experiment. At least 25 images were taken and processed per cell line, time point and pH.

Figure S4: Influence of different host cell environments on spontaneous cystogenesis of *T. gondii*. Human KD3 myoblasts, myotubes and fibroblasts were infected with *T. gondii* Pru-GFP that express GFP under the bradyzoite-specific LDH2-promoter for 96 h. Monolayers were stained with anti-SAG1 antibodies, DBA and DAPI. The GFP signal indicates spontaneous stage conversion to early bradyzoite stages 96 h post-infection in bicarbonate-replete conditions. Scale bar indicates 20 µm.

Figure S5: Immunofluorescence imaging of maturing Pru-tdTomato encysted bradyzoites in KD3 myotubes. Human KD3 myotubes were infected with Pru-tdTomato tachyzoites under

bradyzoite inducing conditions for indicated times and stained with DBA and DAPI. Shown are representative images of 7-, 14-, 21- and 28-day-old Pru-tdTomato tissue cysts. Scale bar indicates 20 µm.

Fig S6: Weight loss and survival of mice infected with Pru-tdTomato tachyzoites and tissue cysts. (A.-B.) Mice were orally infected with either $1x10^4$ myotube (MT)- or human fibroblast (HFF)-derived tachyzoites, 50 or 500 *in vitro*-generated or 10 *in vivo*-generated tissue cysts for 30 days. (A.) The relative weight loss displayed in %. Each data point represents the means of two experiments consisting of five infected animals per group with ± SEM. (B.) % of surviving animals during infection period.

Figure S7: Impact of HDQ treatment on bradyzoite membrane potential and vitality. (A.-B.) Human KD3 myotubes were infected with ME49 tachyzoites under bradyzoite inducing conditions for 28 days, treated for seven days with either 0.005 % DMSO as solvent control or indicated concentration of HDQ and stained with Mitotracker™ Deep Red, DBA and DAPI. Images of 22 cysts per group from two experimental replicates were randomly recorded at identical exposure times. DBA was used to determine the outline of the cysts (green dashed line). For determination of mitochondrial activity, images were converted into monochromatic images and thresholds were set for grey values. We normalized the Mitotracker™ signal (23 to 255) by that of DAPI (19 to 255) per tissue cyst. Values are expressed as means and SEM from two independent experiments. (****p≤0.0001, Mann-Whitney-U-test). Scale bar indicated 10 µm. (C.) Resistance scores of 28-day-old Pru-tdTomato bradyzoites treated with indicated concentrations of HDQ or 0.005 % DMSO as solvent control. Shown are means and SEM of two independent experiments for bradyzoites performed in triplicates.

Figure S8: Data curation LC/MS. Samples were analyzed in positive and negative ionization mode separately. The principal component analyses illustrate effects of the data analysis steps. (A.) Positive and negative datasets were combined. (B.) Blanks were subtracted. Metabolites that had a coverage of less than 50 % in at least one sample set were excluded. (C.) Gaps in the dataset were filled with the mean intensity of the sample group of the respective batch. If a metabolite was not detected in sample group the minimal intensity value was used for gap filling. (D.) Metabolites that were prominent within the magnetic bead or host cell background samples were excluded. (E.) To allow statistical comparison of the cyst samples, which were not normalized to parasite numbers, with the tachyzoites samples, the fractional abundances were calculated by dividing each metabolite intensity by the sum of all intensities per sample. (F.) Because the addition of beads to the tachyzoite samples did not play an important role, these controls were omitted from further analysis.

Figure S9: Transcriptomic data of amino acid transporter genes of *T. gondii* from Pittman et al., 2014[68]. Transcripts per kilobase million were downloaded from ToxoDB (http://www.toxodb.org) and analyzed for stage specific regulation by dividing expression values for acute (10 days post infection (d.p.i.)) by chronic infection in mice (28 d.p.i.).

References

1 Tenter, A., Heckeroth, A. & Weiss, L. Toxoplasma gondii: From animals to humans. *International journal for parasitology* **30**, 1217-1258, doi:10.1016/S0020-7519(00)00124-7 (2000).

2 Barrett, M. P., Kyle, D. E., Sibley, L. D., Radke, J. B. & Tarleton, R. L. Protozoan persister-like cells and drug treatment failure. *Nat Rev Microbiol* **17**, 607-620, doi:10.1038/s41579-019-0238-x (2019).

3 Desmonts, G. *et al.* [Epidemiological study on toxoplasmosis: the influence of cooking slaughter-animal meat on the incidence of human infection]. *Rev Fr Etud Clin Biol* **10**, 952-958 (1965).

4 Luft, B. J., Brooks, R. G., Conley, F. K., McCabe, R. E. & Remington, J. S. Toxoplasmic encephalitis in patients with acquired immune deficiency syndrome. *Jama* **252**, 913-917 (1984).

5 Lopatkin, A. J. *et al.* Bacterial metabolic state more accurately predicts antibiotic lethality than growth rate. *Nature microbiology* **4**, 2109-2117, doi:10.1038/s41564-019-0536-0 (2019).

6 MacRae, J. I. *et al.* Mitochondrial metabolism of glucose and glutamine is required for intracellular growth of Toxoplasma gondii. *Cell Host Microbe* **12**, 682-692, doi:10.1016/j.chom.2012.09.013 (2012).

7 Blume, M. *et al.* A Toxoplasma gondii Gluconeogenic Enzyme Contributes to Robust Central Carbon Metabolism and Is Essential for Replication and Virulence. *Cell Host Microbe* **18**, 210-220, doi:10.1016/j.chom.2015.07.008 (2015).

8 Olson, W. J. *et al.* Dual metabolomic profiling uncovers Toxoplasma manipulation of the host metabolome and the discovery of a novel parasite metabolic capability. *PLoS pathogens* **16**, e1008432, doi:10.1371/journal.ppat.1008432 (2020).

9 Blume, M. & Seeber, F. Metabolic interactions between Toxoplasma gondii and its host. *F1000Res* **7**, doi:10.12688/f1000research.16021.1 (2018).

10 Murata, Y., Sugi, T., Weiss, L. M. & Kato, K. Identification of compounds that suppress Toxoplasma gondii tachyzoites and bradyzoites. *PLoS One* **12**, e0178203, doi:10.1371/journal.pone.0178203 (2017).

11 Shukla, A. *et al.* Glycolysis is important for optimal asexual growth and formation of mature tissue cysts by Toxoplasma gondii. *Int J Parasitol* **48**, 955-968, doi:10.1016/j.ijpara.2018.05.013 (2018).

12 Abdelbaset, A. E. *et al.* Lactate dehydrogenase in Toxoplasma gondii controls virulence, bradyzoite differentiation, and chronic infection. *PLoS One* **12**, e0173745, doi:10.1371/journal.pone.0173745 (2017).

13 Tomavo, S. & Boothroyd, J. C. Interconnection between organellar functions, development and drug resistance in the protozoan parasite, Toxoplasma gondii. *Int J Parasitol* **25**, 1293-1299, doi:10.1016/0020-7519(95)00066-b (1995).

14 Ferreira da Silva Mda, F., Barbosa, H. S., Gross, U. & Lüder, C. G. Stress-related and spontaneous stage differentiation of Toxoplasma gondii. *Mol Biosyst* **4**, 824-834, doi:10.1039/b800520f (2008).

15 Araujo, F. G., Huskinson, J. & Remington, J. S. Remarkable in vitro and in vivo activities of the hydroxynaphthoquinone 566C80 against tachyzoites and tissue cysts of Toxoplasma gondii. *Antimicrob Agents Chemother* **35**, 293-299, doi:10.1128/aac.35.2.293 (1991).

16 Ferguson, D. J., Huskinson-Mark, J., Araujo, F. G. & Remington, J. S. An ultrastructural study of the effect of treatment with atovaquone in brains of mice chronically infected with the ME49 strain of Toxoplasma gondii. *Int J Exp Pathol* **75**, 111-116 (1994).

17 Araujo, F. G., Huskinson-Mark, J., Gutteridge, W. E. & Remington, J. S. In vitro and in vivo activities of the hydroxynaphthoquinone 566C80 against the cyst form of Toxoplasma gondii. *Antimicrob Agents Chemother* **36**, 326-330, doi:10.1128/aac.36.2.326 (1992).

18 Di Cristina, M. *et al.* Toxoplasma depends on lysosomal consumption of autophagosomes for persistent infection. *Nature microbiology* **2**, 17096, doi:10.1038/nmicrobiol.2017.96 (2017).

19 Smith, D. *et al.* Toxoplasma TgATG9 is critical for autophagy and long-term persistence in tissue cysts. *bioRxiv*, 2020.2005.2013.093401, doi:10.1101/2020.05.13.093401 (2020).

20 Lüder, C. G. K. & Rahman, T. Impact of the host on Toxoplasma stage differentiation. *Microb Cell* **4**, 203-211, doi:10.15698/mic2017.07.579 (2017).

21 Ferguson, D. J. & Hutchison, W. M. An ultrastructural study of the early development and tissue cyst formation of Toxoplasma gondii in the brains of mice. *Parasitol Res* **73**, 483-491, doi:10.1007/bf00535321 (1987).

22 Watts, E. *et al.* Novel Approaches Reveal that Toxoplasma gondii Bradyzoites within Tissue Cysts Are Dynamic and Replicating Entities In Vivo. *MBio* **6**, e01155-01115, doi:10.1128/mBio.01155-15 (2015).

23 Soete, M., Camus, D. & Dubremetz, J. F. Experimental induction of bradyzoite-specific antigen expression and cyst formation by the RH strain of Toxoplasma gondii in vitro. *Exp Parasitol* **78**, 361-370, doi:10.1006/expr.1994.1039 (1994).

24 Fox, B. A., Gigley, J. P. & Bzik, D. J. Toxoplasma gondii lacks the enzymes required for de novo arginine biosynthesis and arginine starvation triggers cyst formation. *Int J Parasitol* **34**, 323-331, doi:10.1016/j.ijpara.2003.12.001 (2004).

25 Mahamed, D. A., Mills, J. H., Egan, C. E., Denkers, E. Y. & Bynoe, M. S. CD73-generated adenosine facilitates Toxoplasma gondii differentiation to long-lived tissue cysts in the central nervous system. *Proceedings of the National Academy of Sciences of the United States of America* **109**, 16312-16317, doi:10.1073/pnas.1205589109 (2012).

26 Donald, R. G. *et al.* Toxoplasma gondii cyclic GMP-dependent kinase: chemotherapeutic targeting of an essential parasite protein kinase. *Eukaryot Cell* **1**, 317-328, doi:10.1128/ec.1.3.317-328.2002 (2002).

27 Weilhammer, D. R. *et al.* Host metabolism regulates growth and differentiation of Toxoplasma gondii. *International Journal for Parasitology* **42**, 947-959, doi:https://doi.org/10.1016/j.ijpara.2012.07.011 (2012).

28 Mayoral, J., Di Cristina, M., Carruthers, V. B. & Weiss, L. M. Toxoplasma gondii: Bradyzoite Differentiation In Vitro and In Vivo. *Methods Mol Biol* **2071**, 269-282, doi:10.1007/978-1-4939-9857-9_15 (2020).

29 Guimaraes, E. V., de Carvalho, L. & Barbosa, H. S. Primary culture of skeletal muscle cells as a model for studies of Toxoplasma gondii cystogenesis. *J Parasitol* **94**, 72-83, doi:10.1645/GE-1273.1 (2008).

30 Guimarães, E. V., Carvalho, L. d. & Barbosa, H. S. Interaction and cystogenesis of Toxoplasma gondii within skeletal muscle cells in vitro. *Memórias do Instituto Oswaldo Cruz* **104**, 170-174 (2009).

31 Mouveaux, T. *et al.* Primary brain cell infection by Toxoplasma gondii reveals the extent and dynamics of parasite differentiation and its impact on neuron biology. *Open biology* **11**, 210053, doi:10.1098/rsob.210053 (2021).

32 Fux, B. *et al.* Toxoplasma gondii Strains Defective in Oral Transmission Are Also Defective in Developmental Stage Differentiation. *Infection and immunity* **75**, 2580-2590, doi:10.1128/IAI.00085-07 (2007).

33 Dubey, J. P., Kotula, A. W., Sharar, A., Andrews, C. D. & Lindsay, D. S. Effect of high temperature on infectivity of Toxoplasma gondii tissue cysts in pork. *J Parasitol* **76**, 201-204 (1990).
34 Dunay, I. R., Gajurel, K., Dhakal, R., Liesenfeld, O. & Montoya, J. G. Treatment of Toxoplasmosis: Historical Perspective, Animal Models, and Current Clinical Practice. *Clin Microbiol Rev* **31**, doi:10.1128/cmr.00057-17 (2018).
35 Shiomi, K. *et al.* CDK4 and cyclin D1 allow human myogenic cells to recapture growth property without compromising differentiation potential. *Gene Ther* **18**, 857-866, doi:10.1038/gt.2011.44 (2011).
36 Sabin, A. B. Toxoplasmic Encephalitis In Children. *JAMA* **116**, 801-807, doi:10.1001/jama.1941.02820090001001 (1941).
37 Huynh, M.-H. & Carruthers, V. B. Tagging of endogenous genes in a Toxoplasma gondii strain lacking Ku80. *Eukaryotic cell* **8**, 530-539, doi:10.1128/EC.00358-08 (2009).
38 Dubey, J. P. Mouse pathogenicity of Toxoplasma gondii isolated from a goat. *Am J Vet Res* **41**, 427-429 (1980).
39 Guo, Z.-G., Gross, U. & Johnson, A. M. Toxoplasma gondii virulence markers identified by random amplified polymorphic DNA polymerase chain reaction. *Parasitology Research* **83**, 458-463, doi:10.1007/s004360050280 (1997).
40 Singh, U., Brewer, J. L. & Boothroyd, J. C. Genetic analysis of tachyzoite to bradyzoite differentiation mutants in Toxoplasma gondii reveals a hierarchy of gene induction. *Mol Microbiol* **44**, 721-733, doi:10.1046/j.1365-2958.2002.02903.x (2002).
41 Chtanova, T. *et al.* Dynamics of neutrophil migration in lymph nodes during infection. *Immunity* **29**, 487-496, doi:10.1016/j.immuni.2008.07.012 (2008).
42 Darde, M. L., Bouteille, B. & Pestre-Alexandre, M. Isoenzyme analysis of 35 Toxoplasma gondii isolates and the biological and epidemiological implications. *J Parasitol* **78**, 786-794 (1992).
43 Sibley, L. D., Mordue, D. G., Su, C., Robben, P. M. & Howe, D. K. Genetic approaches to studying virulence and pathogenesis in Toxoplasma gondii. *Philos Trans R Soc Lond B Biol Sci* **357**, 81-88, doi:10.1098/rstb.2001.1017 (2002).
44 Laue, M. Electron microscopy of viruses. *Methods in cell biology* **96**, 1-20, doi:10.1016/s0091-679x(10)96001-9 (2010).
45 Gross, U. *et al.* Monoclonal rat antibodies directed against Toxoplasma gondii suitable for studying tachyzoite-bradyzoite interconversion in vivo. *Clin Diagn Lab Immunol* **2**, 542-548 (1995).
46 Bulow, R. & Boothroyd, J. C. Protection of mice from fatal Toxoplasma gondii infection by immunization with p30 antigen in liposomes. *J Immunol* **147**, 3496-3500 (1991).
47 Schneider, C. A., Rasband, W. S. & Eliceiri, K. W. NIH Image to ImageJ: 25 years of image analysis. *Nat Methods* **9**, 671-675 (2012).
48 Dubey, J. P. Re-examination of resistance of Toxoplasma gondii tachyzoites and bradyzoites to pepsin and trypsin digestion. *Parasitology* **116 (Pt 1)**, 43-50 (1998).
49 Matta, S. K. *et al.* Toxoplasma gondii effector TgIST blocks type I interferon signaling to promote infection. *Proceedings of the National Academy of Sciences of the United States of America* **116**, 17480-17491, doi:10.1073/pnas.1904637116 (2019).
50 Huang, W. *et al.* SAR Studies of 5-Aminopyrazole-4-carboxamide Analogues as Potent and Selective Inhibitors of Toxoplasma gondii CDPK1. *ACS Med Chem Lett* **6**, 1184-1189, doi:10.1021/acsmedchemlett.5b00319 (2015).
51 Doggett, J. S., Ojo, K. K., Fan, E., Maly, D. J. & Van Voorhis, W. C. Bumped kinase inhibitor 1294 treats established Toxoplasma gondii infection. *Antimicrobial agents and chemotherapy* **58**, 3547-3549, doi:10.1128/AAC.01823-13 (2014).

52 Metsalu, T. & Vilo, J. ClustVis: a web tool for visualizing clustering of multivariate data using Principal Component Analysis and heatmap. *Nucleic acids research* **43**, W566-570, doi:10.1093/nar/gkv468 (2015).
53 Dubey, J. P. Long-term persistence of Toxoplasma gondii in tissues of pigs inoculated with T gondii oocysts and effect of freezing on viability of tissue cysts in pork. *Am J Vet Res* **49**, 910-913 (1988).
54 Speer, C. A., Dubey, J. P., McAllister, M. M. & Blixt, J. A. Comparative ultrastructure of tachyzoites, bradyzoites, and tissue cysts of Neospora caninum and Toxoplasma gondii. *Int J Parasitol* **29**, 1509-1519, doi:10.1016/s0020-7519(99)00132-0 (1999).
55 Sullivan, W. J., Jr., Smith, A. T. & Joyce, B. R. Understanding mechanisms and the role of differentiation in pathogenesis of Toxoplasma gondii: a review. *Mem Inst Oswaldo Cruz* **104**, 155-161, doi:10.1590/s0074-02762009000200005 (2009).
56 Ferguson, D. J. Use of molecular and ultrastructural markers to evaluate stage conversion of Toxoplasma gondii in both the intermediate and definitive host. *Int J Parasitol* **34**, 347-360, doi:10.1016/j.ijpara.2003.11.024 (2004).
57 Ferreira-da-Silva Mda, F., Takacs, A. C., Barbosa, H. S., Gross, U. & Lüder, C. G. Primary skeletal muscle cells trigger spontaneous Toxoplasma gondii tachyzoite-to-bradyzoite conversion at higher rates than fibroblasts. *Int J Med Microbiol* **299**, 381-388, doi:10.1016/j.ijmm.2008.10.002 (2009).
58 Hegewald, J., Gross, U. & Bohne, W. Identification of dihydroorotate dehydrogenase as a relevant drug target for 1-hydroxyquinolones in Toxoplasma gondii. *Mol Biochem Parasitol* **190**, 6-15, doi:10.1016/j.molbiopara.2013.05.008 (2013).
59 Saleh, A., Friesen, J., Baumeister, S., Gross, U. & Bohne, W. Growth inhibition of Toxoplasma gondii and Plasmodium falciparum by nanomolar concentrations of 1-hydroxy-2-dodecyl-4(1H)quinolone, a high-affinity inhibitor of alternative (type II) NADH dehydrogenases. *Antimicrob Agents Chemother* **51**, 1217-1222, doi:10.1128/aac.00895-06 (2007).
60 Winzer, P. *et al.* In Vitro and In Vivo Effects of the Bumped Kinase Inhibitor 1294 in the Related Cyst-Forming Apicomplexans Toxoplasma gondii and Neospora caninum. *Antimicrob Agents Chemother* **59**, 6361-6374, doi:10.1128/aac.01236-15 (2015).
61 Scheele, S. *et al.* Toxoplasma Calcium-Dependent Protein Kinase 1 Inhibitors: Probing Activity and Resistance Using Cellular Thermal Shift Assays. *Antimicrob Agents Chemother* **62**, doi:10.1128/AAC.00051-18 (2018).
62 Tomita, T. *et al.* The Toxoplasma gondii cyst wall protein CST1 is critical for cyst wall integrity and promotes bradyzoite persistence. *PLoS pathogens* **9**, e1003823, doi:10.1371/journal.ppat.1003823 (2013).
63 Cerutti, A., Blanchard, N. & Besteiro, S. The Bradyzoite: A Key Developmental Stage for the Persistence and Pathogenesis of Toxoplasmosis. *Pathogens* **9**, doi:10.3390/pathogens9030234 (2020).
64 Denton, H., Roberts, C. W., Alexander, J., Thong, K. W. & Coombs, G. H. Enzymes of energy metabolism in the bradyzoites and tachyzoites of Toxoplasma gondii. *FEMS microbiology letters* **137**, 103-108, doi:10.1111/j.1574-6968.1996.tb08090.x (1996).
65 Fleige, T., Pfaff, N., Gross, U. & Bohne, W. Localisation of gluconeogenesis and tricarboxylic acid (TCA)-cycle enzymes and first functional analysis of the TCA cycle in Toxoplasma gondii. *Int J Parasitol* **38**, 1121-1132, doi:10.1016/j.ijpara.2008.01.007 (2008).
66 Lin, S. S. *et al.* The Toxoplasma gondii type-II NADH dehydrogenase TgNDH2-I is inhibited by 1-hydroxy-2-alkyl-4(1H)quinolones. *Biochimica et biophysica acta* **1777**, 1455-1462, doi:10.1016/j.bbabio.2008.08.006 (2008).

67 Sugi, T., Tu, V., Ma, Y., Tomita, T. & Weiss, L. M. Toxoplasma gondii Requires Glycogen Phosphorylase for Balancing Amylopectin Storage and for Efficient Production of Brain Cysts. *MBio* **8**, doi:10.1128/mBio.01289-17 (2017).
68 Xia, N. *et al.* A Lactate Fermentation Mutant of Toxoplasma Stimulates Protective Immunity Against Acute and Chronic Toxoplasmosis. *Front Immunol* **9**, 1814, doi:10.3389/fimmu.2018.01814 (2018).
69 Pittman, K. J., Aliota, M. T. & Knoll, L. J. Dual transcriptional profiling of mice and Toxoplasma gondii during acute and chronic infection. *BMC genomics* **15**, 806, doi:10.1186/1471-2164-15-806 (2014).
70 Bertschi, N. L. *et al.* Transcriptomic analysis reveals reduced transcriptional activity in the malaria parasite Plasmodium cynomolgi during progression into dormancy. *Elife* **7**, doi:10.7554/eLife.41081 (2018).
71 Krishnan, A. *et al.* Functional and Computational Genomics Reveal Unprecedented Flexibility in Stage-Specific Toxoplasma Metabolism. *Cell Host Microbe* **27**, 290-306.e211, doi:10.1016/j.chom.2020.01.002 (2020).
72 Parker, K. E. R. *et al.* The tyrosine transporter of Toxoplasma gondii is a member of the newly defined apicomplexan amino acid transporter (ApiAT) family. *PLoS pathogens* **15**, e1007577, doi:10.1371/journal.ppat.1007577 (2019).
73 Jeffers, V., Tampaki, Z., Kim, K. & Sullivan, W. J., Jr. A latent ability to persist: differentiation in Toxoplasma gondii. *Cell Mol Life Sci* **75**, 2355-2373, doi:10.1007/s00018-018-2808-x (2018).
74 Dou, Z., McGovern, O. L., Di Cristina, M. & Carruthers, V. B. Toxoplasma gondii ingests and digests host cytosolic proteins. *mBio* **5**, e01188-01114, doi:10.1128/mBio.01188-14 (2014).
75 Sullivan, W. J., Jr., Narasimhan, J., Bhatti, M. M. & Wek, R. C. Parasite-specific eIF2 (eukaryotic initiation factor-2) kinase required for stress-induced translation control. *The Biochemical journal* **380**, 523-531, doi:10.1042/bj20040262 (2004).
76 Saunders, E. C. *et al.* Induction of a stringent metabolic response in intracellular stages of Leishmania mexicana leads to increased dependence on mitochondrial metabolism. *PLoS pathogens* **10**, e1003888, doi:10.1371/journal.ppat.1003888 (2014).
77 Fox, B. A. & Bzik, D. J. De novo pyrimidine biosynthesis is required for virulence of Toxoplasma gondii. *Nature* **415**, 926-929, doi:10.1038/415926a (2002).
78 Chiang, C. W. *et al.* The adenosine transporter of Toxoplasma gondii. Identification by insertional mutagenesis, cloning, and recombinant expression. *J Biol Chem* **274**, 35255-35261, doi:10.1074/jbc.274.49.35255 (1999).
79 De Koning, H. P., Al-Salabi, M. I., Cohen, A. M., Coombs, G. H. & Wastling, J. M. Identification and characterisation of high affinity nucleoside and nucleobase transporters in Toxoplasma gondii. *International Journal for Parasitology* **33**, 821-831, doi:https://doi.org/10.1016/S0020-7519(03)00091-2 (2003).
80 Fox, B. A. *et al.* Type II Toxoplasma gondii KU80 knockout strains enable functional analysis of genes required for cyst development and latent infection. *Eukaryot Cell* **10**, 1193-1206, doi:10.1128/ec.00297-10 (2011).
81 Painter, H. J., Morrisey, J. M., Mather, M. W. & Vaidya, A. B. Specific role of mitochondrial electron transport in blood-stage Plasmodium falciparum. *Nature* **446**, 88-91, doi:10.1038/nature05572 (2007).
82 Hortua Triana, M. A. *et al.* Biochemical and molecular characterization of the pyrimidine biosynthetic enzyme dihydroorotate dehydrogenase from Toxoplasma gondii. *Mol Biochem Parasitol* **184**, 71-81, doi:10.1016/j.molbiopara.2012.04.009 (2012).
83 Lin, S. S., Gross, U. & Bohne, W. Type II NADH dehydrogenase inhibitor 1-hydroxy-2-dodecyl-4(1H)quinolone leads to collapse of mitochondrial inner-membrane potential

and ATP depletion in Toxoplasma gondii. *Eukaryot Cell* **8**, 877-887, doi:10.1128/EC.00381-08 (2009).

84 Doggett, J. S. *et al.* Endochin-like quinolones are highly efficacious against acute and latent experimental toxoplasmosis. *Proceedings of the National Academy of Sciences of the United States of America* **109**, 15936-15941, doi:10.1073/pnas.1208069109 (2012).

85 Malinska, D., Kudin, A. P., Bejtka, M. & Kunz, W. S. Changes in mitochondrial reactive oxygen species synthesis during differentiation of skeletal muscle cells. *Mitochondrion* **12**, 144-148, doi:10.1016/j.mito.2011.06.015 (2012).

86 Radke, J. R. *et al.* Changes in the expression of human cell division autoantigen-1 influence Toxoplasma gondii growth and development. *PLoS pathogens* **2**, e105, doi:10.1371/journal.ppat.0020105 (2006).

87 Swierzy, I. J. & Lüder, C. G. K. Withdrawal of skeletal muscle cells from cell cycle progression triggers differentiation of Toxoplasma gondii towards the bradyzoite stage. *Cellular Microbiology* **17**, 2-17, doi:10.1111/cmi.12342 (2015).

88 Roos, D. S. Primary structure of the dihydrofolate reductase-thymidylate synthase gene from Toxoplasma gondii. *J Biol Chem* **268**, 6269-6280 (1993).

89 Bajohr, L. L. *et al.* In vitro and in vivo activities of 1-hydroxy-2-alkyl-4(1H)quinolone derivatives against Toxoplasma gondii. *Antimicrob Agents Chemother* **54**, 517-521, doi:10.1128/AAC.01001-09 (2010).

90 Ferguson, D. J., Huskinson-Mark, J., Araujo, F. G. & Remington, J. S. A morphological study of chronic cerebral toxoplasmosis in mice: comparison of four different strains of Toxoplasma gondii. *Parasitol Res* **80**, 493-501, doi:10.1007/bf00932696 (1994).

91 Yap, G. S. *et al.* Partially protective vaccination permits the development of latency in a normally virulent strain of Toxoplasma gondii. *Infect Immun* **66**, 4382-4388 (1998).

92 Bakkeren, E., Diard, M. & Hardt, W.-D. Evolutionary causes and consequences of bacterial antibiotic persistence. *Nature Reviews Microbiology* **18**, 479-490, doi:10.1038/s41579-020-0378-z (2020).

Fig. 1

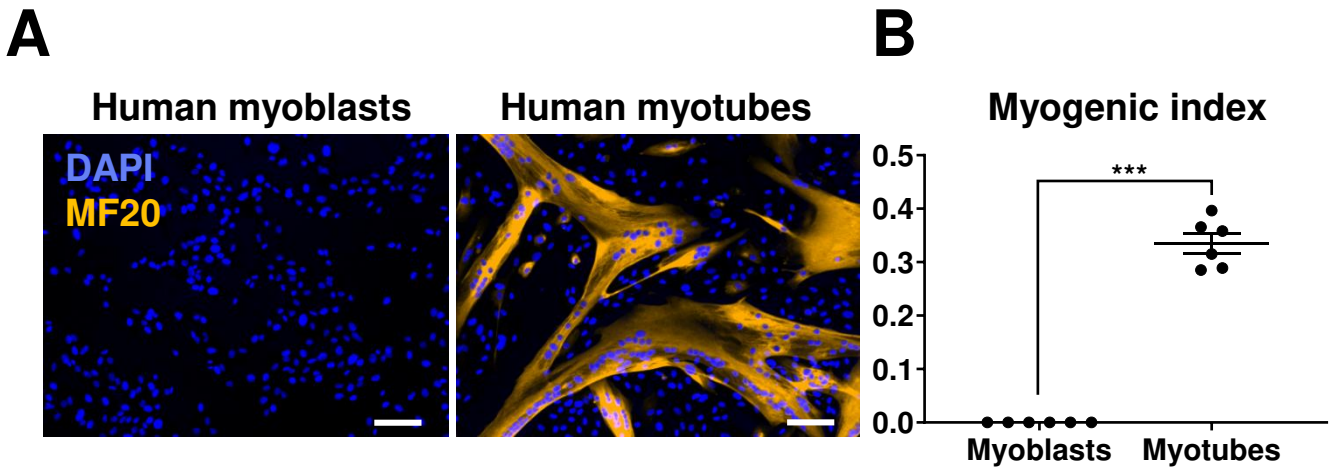

Fig. 2

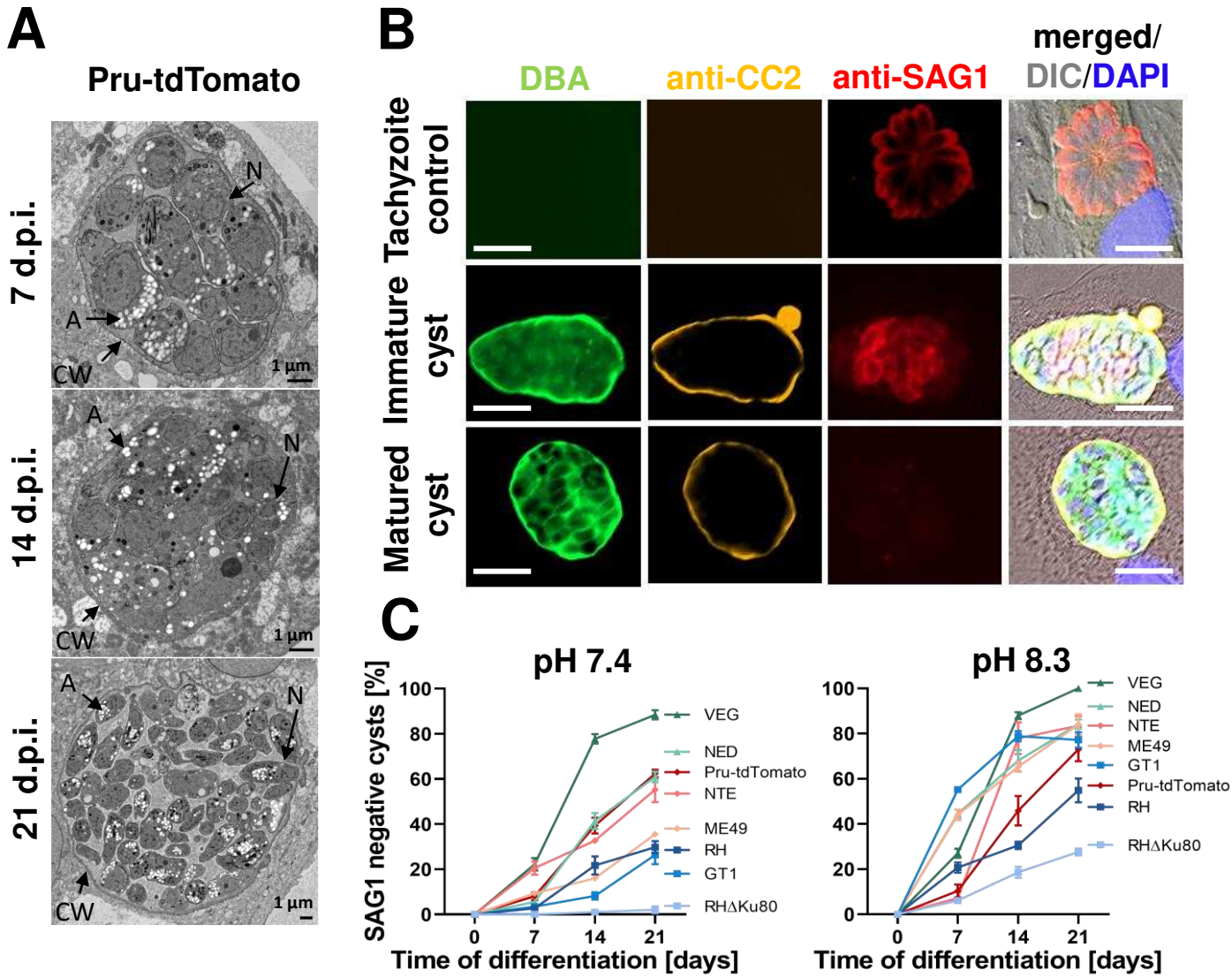

Fig. 3

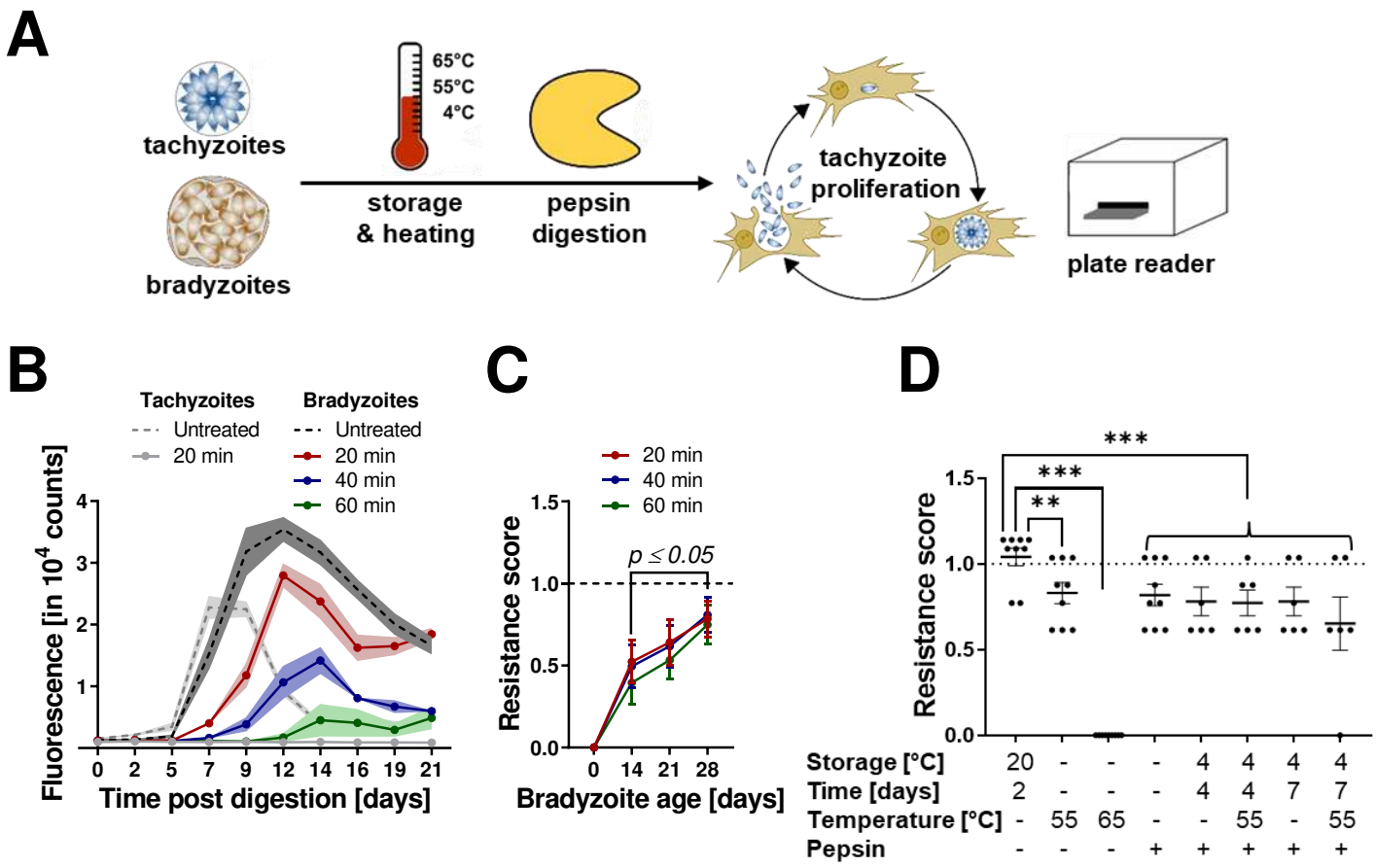

Fig. 4

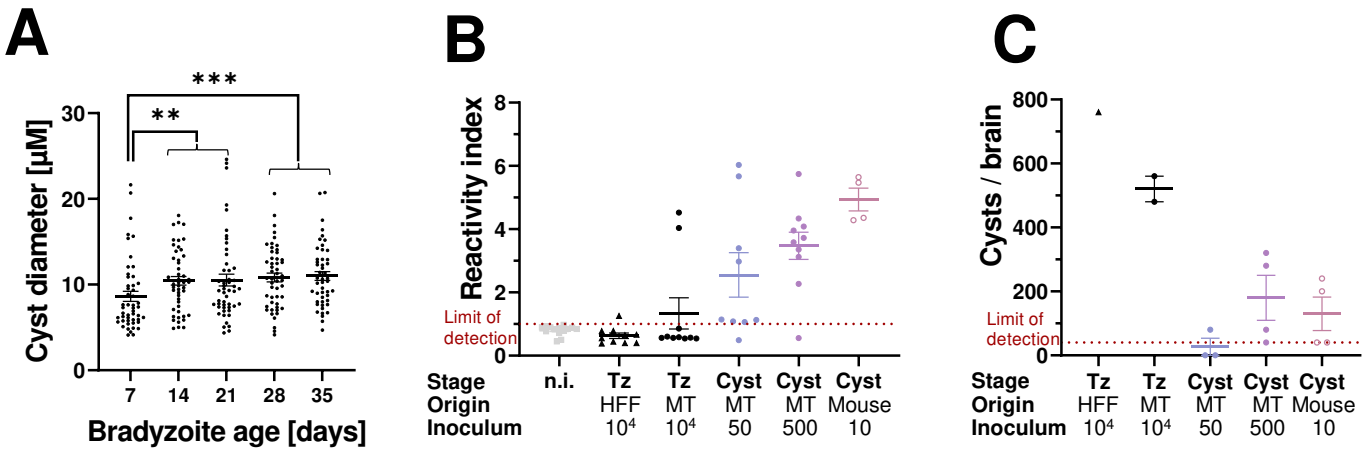

D

Stage	Tz	Tz	Cyst	Cyst	Cyst
Origin	HFF	MT	MT	MT	Mouse
Inoculum	10^4	10^4	50	500	10
Seroconversion	1/10	2/10	8/10†*	9/10†*	4/5†
Brain cysts**	1/1	2/2	1/3	4/4	4/4

Fig. 5

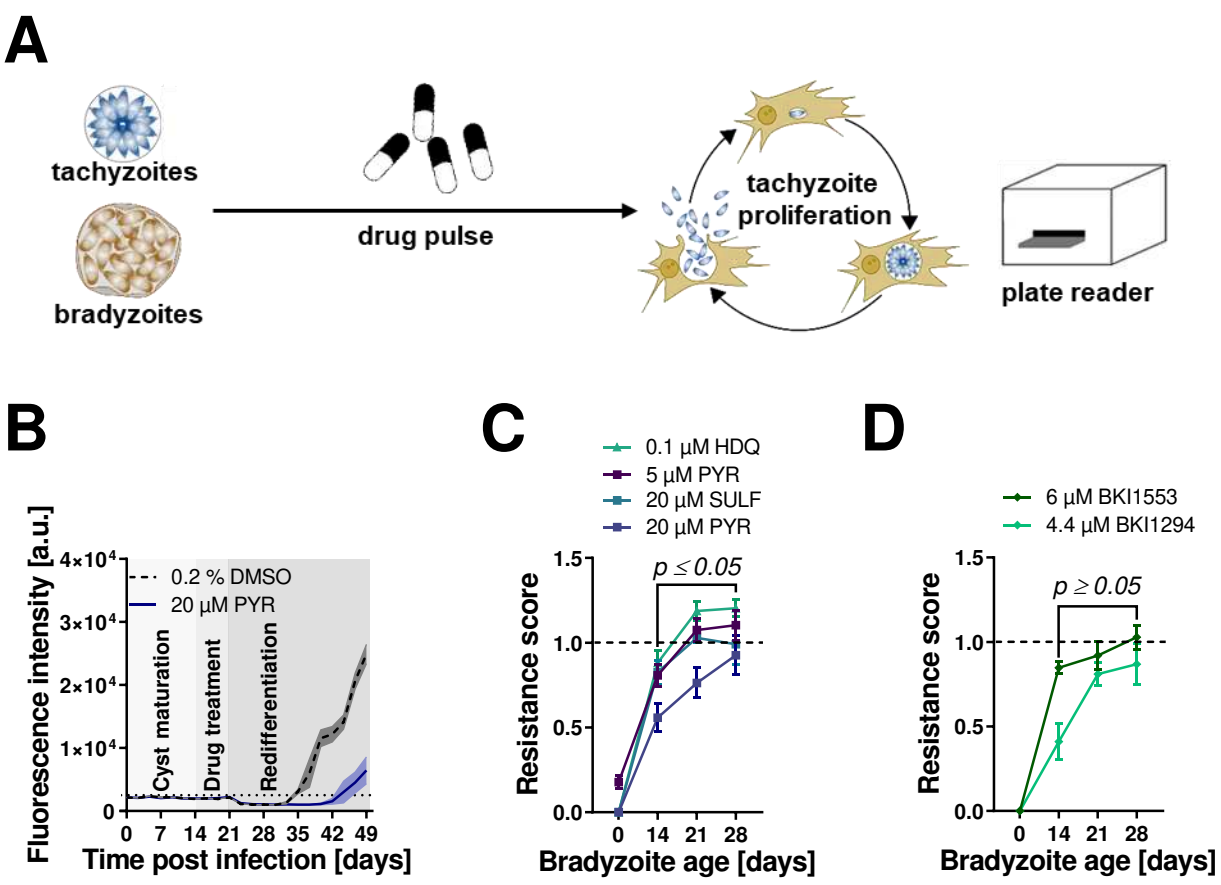

Fig. 6

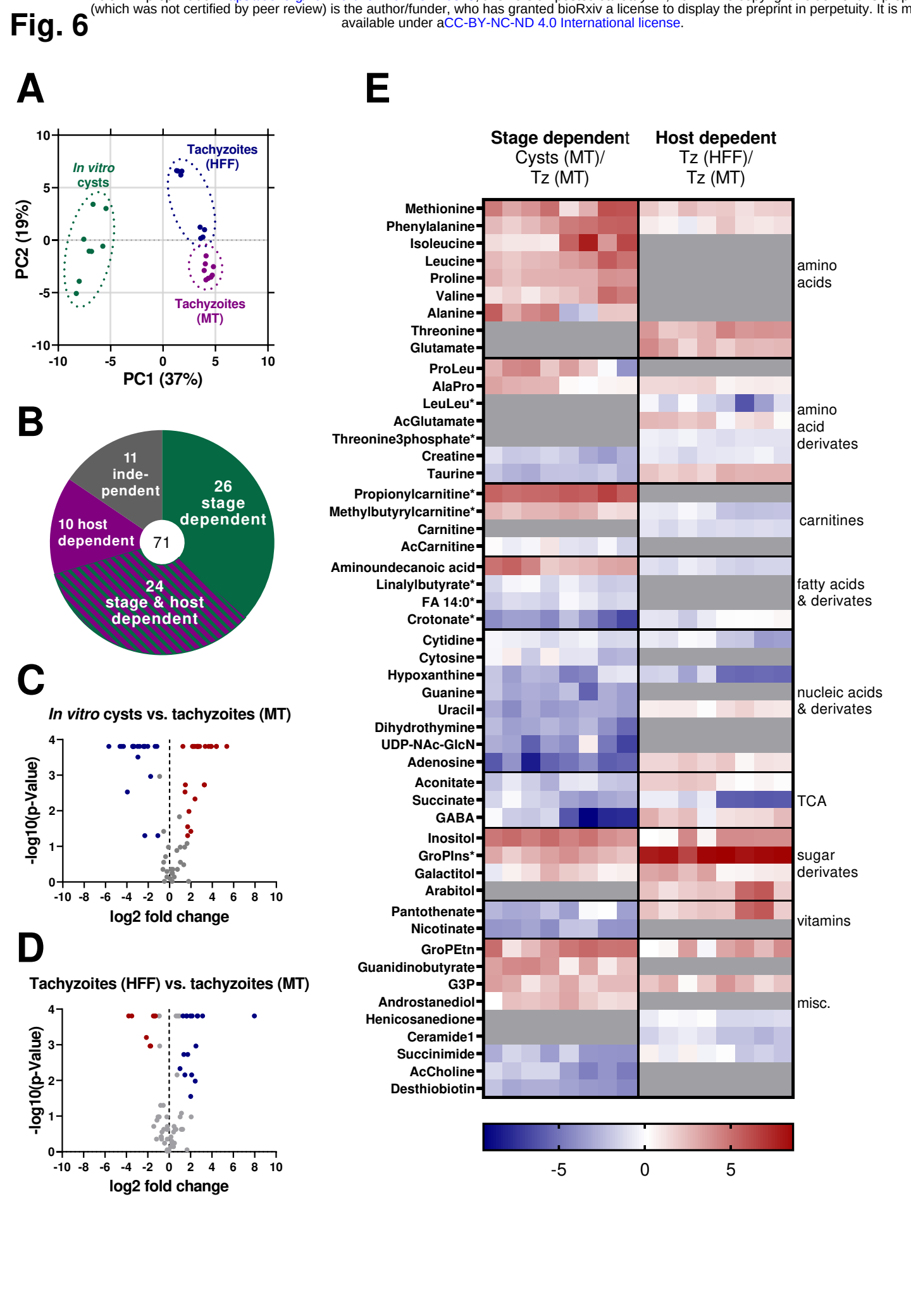

Fig. 7

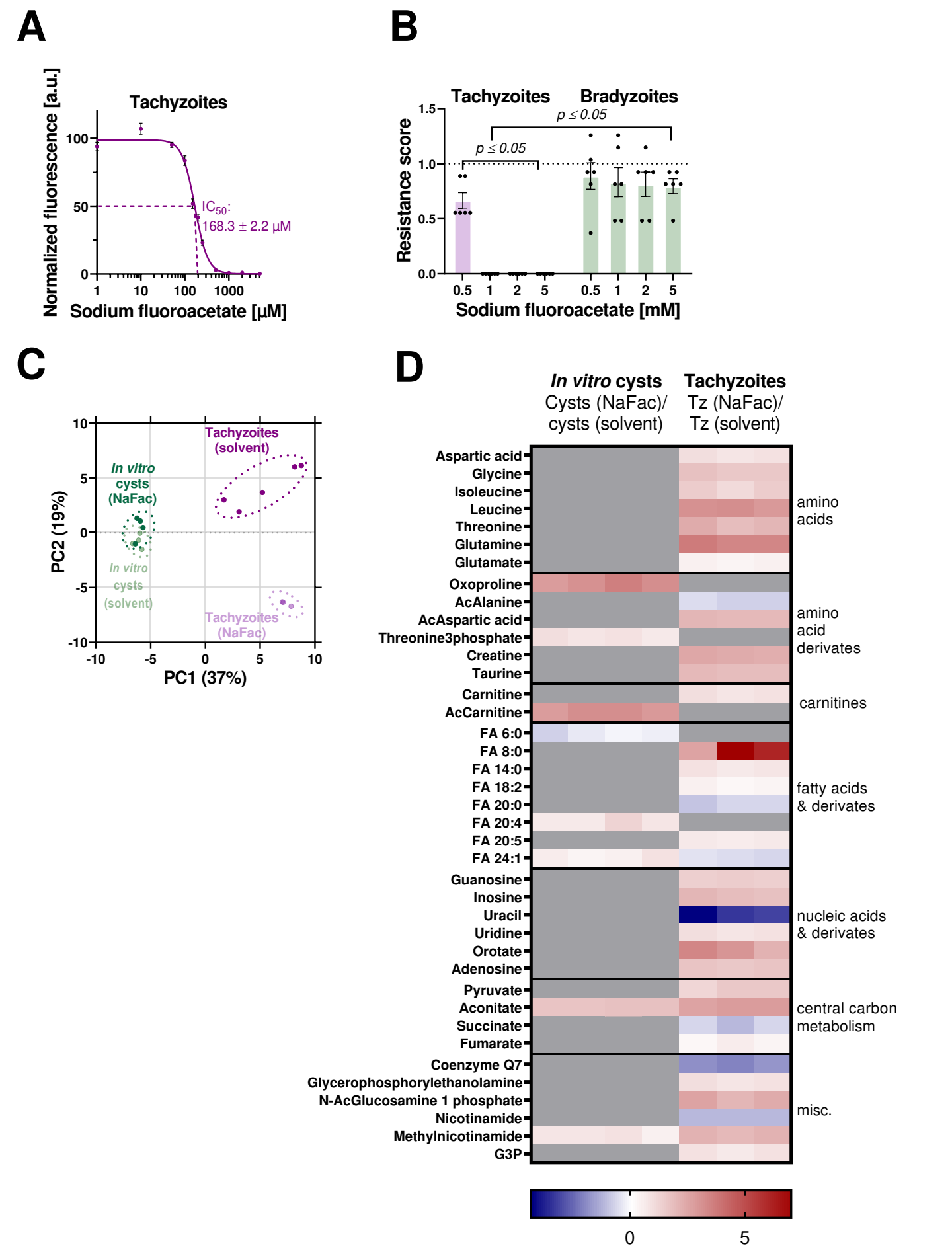

Fig. S1

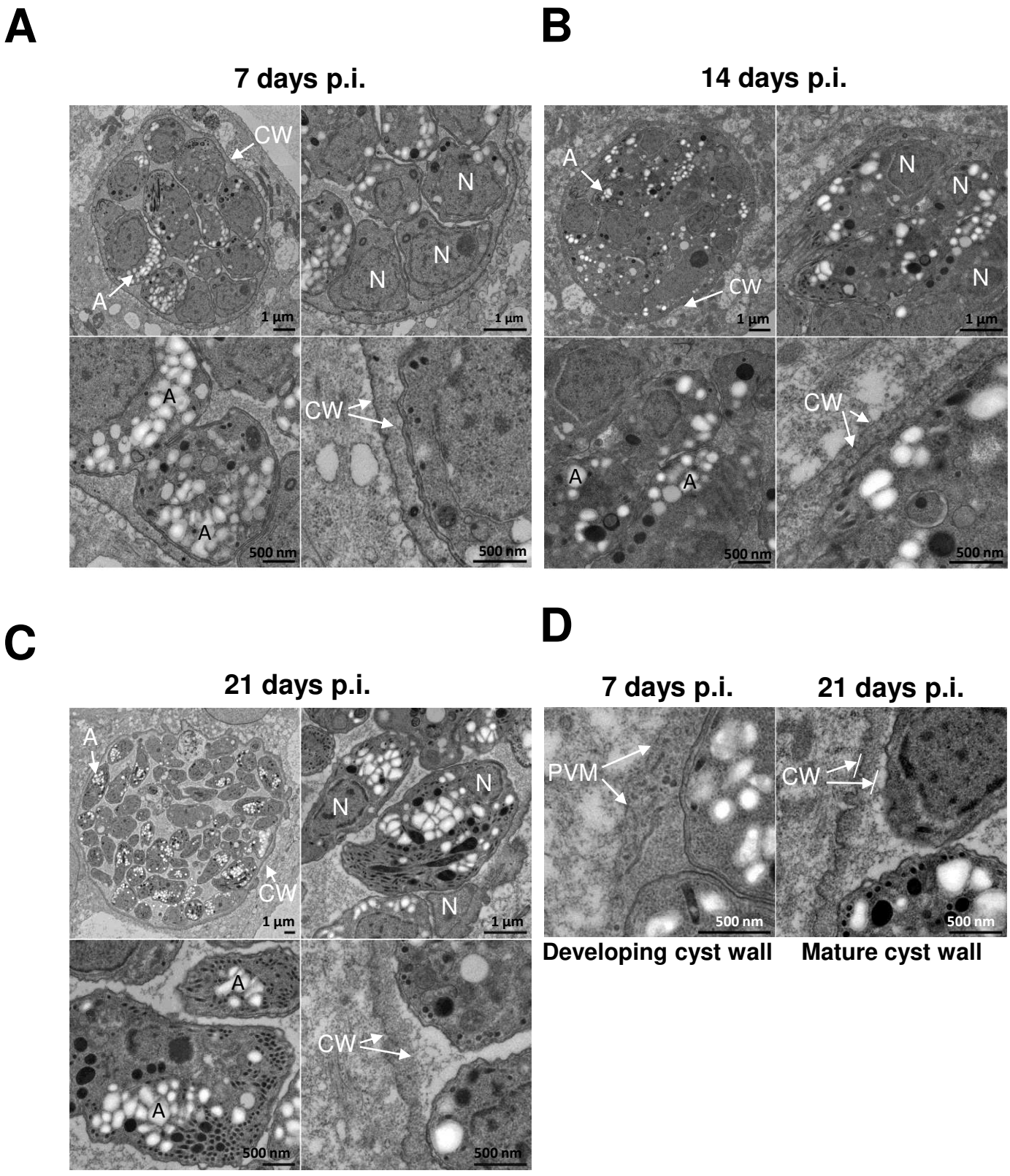

Fig. S2

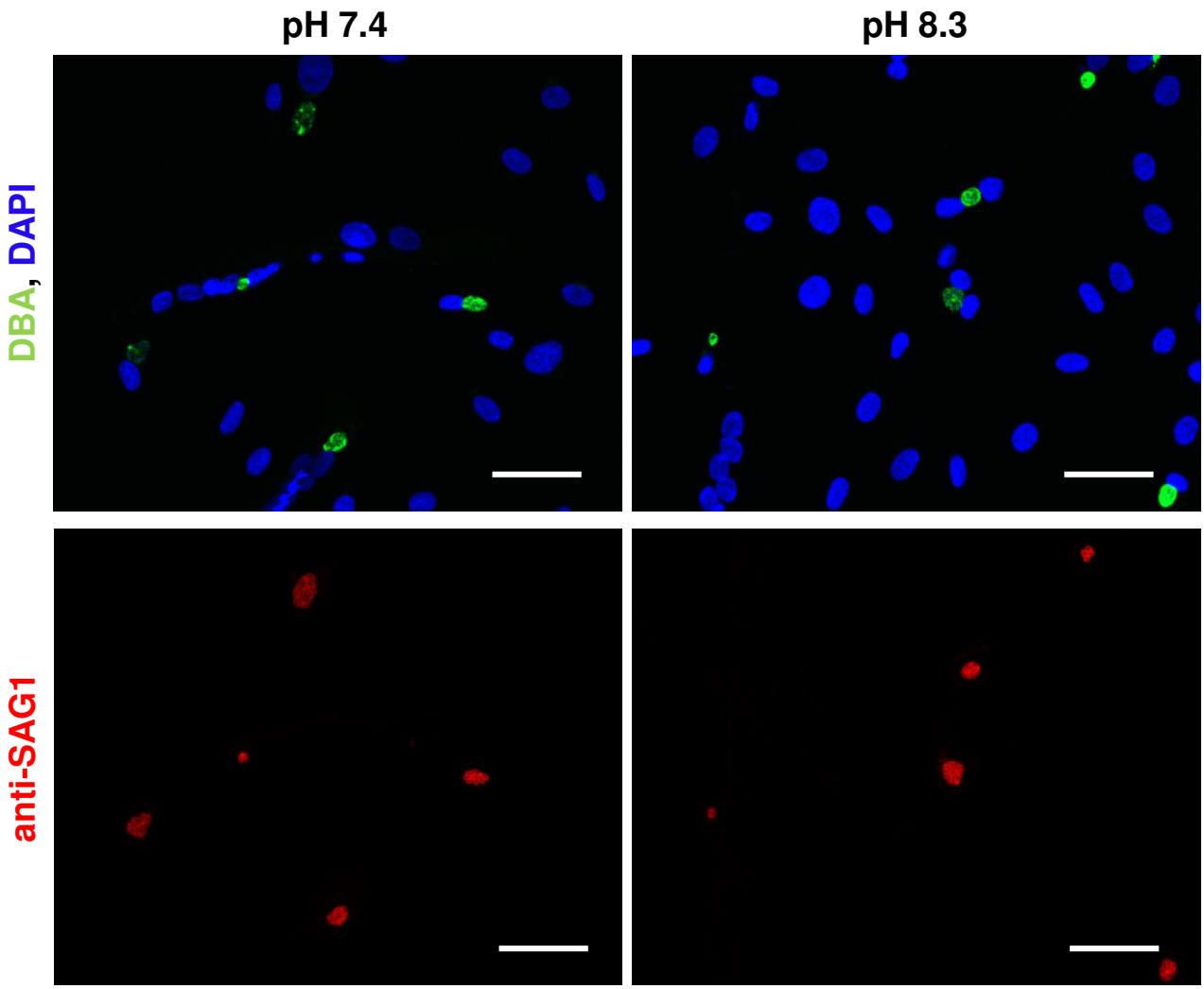

Fig. S3

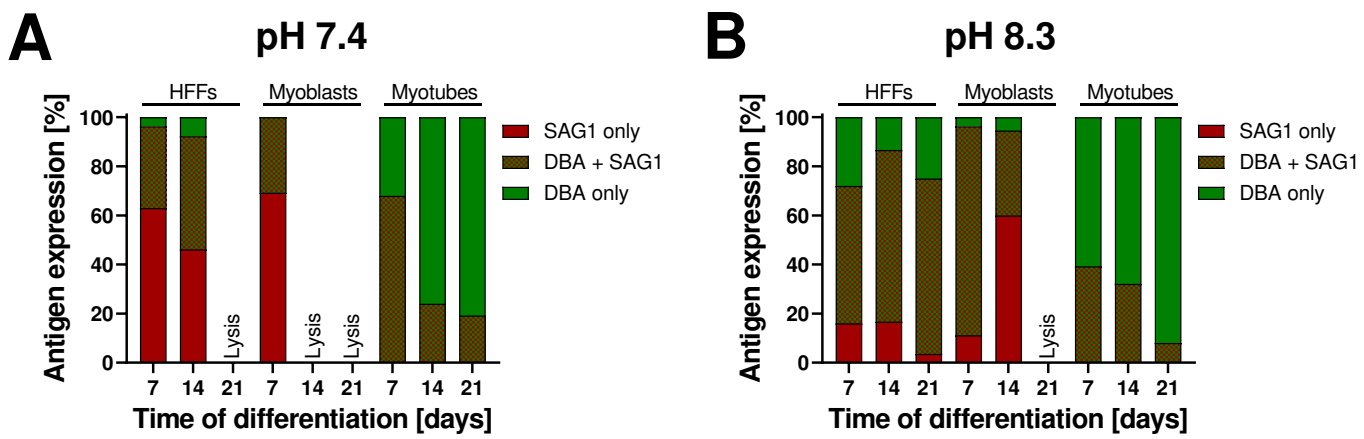

Fig. S4

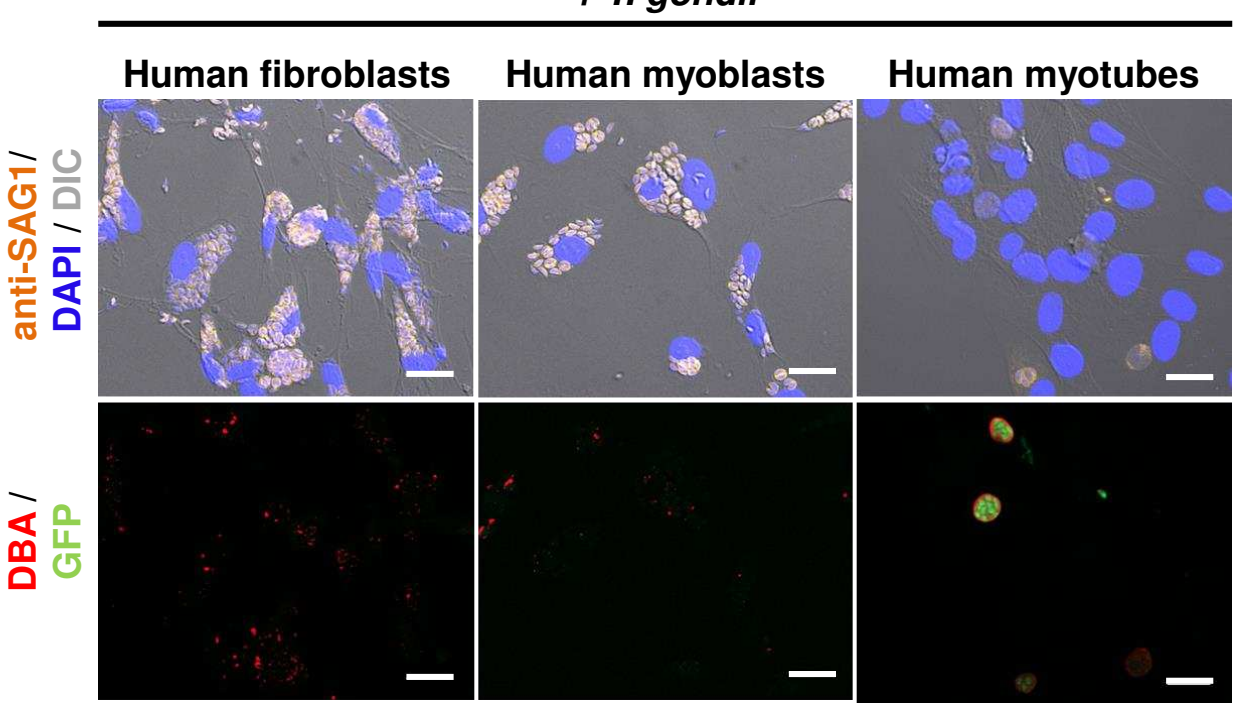

Fig. S5

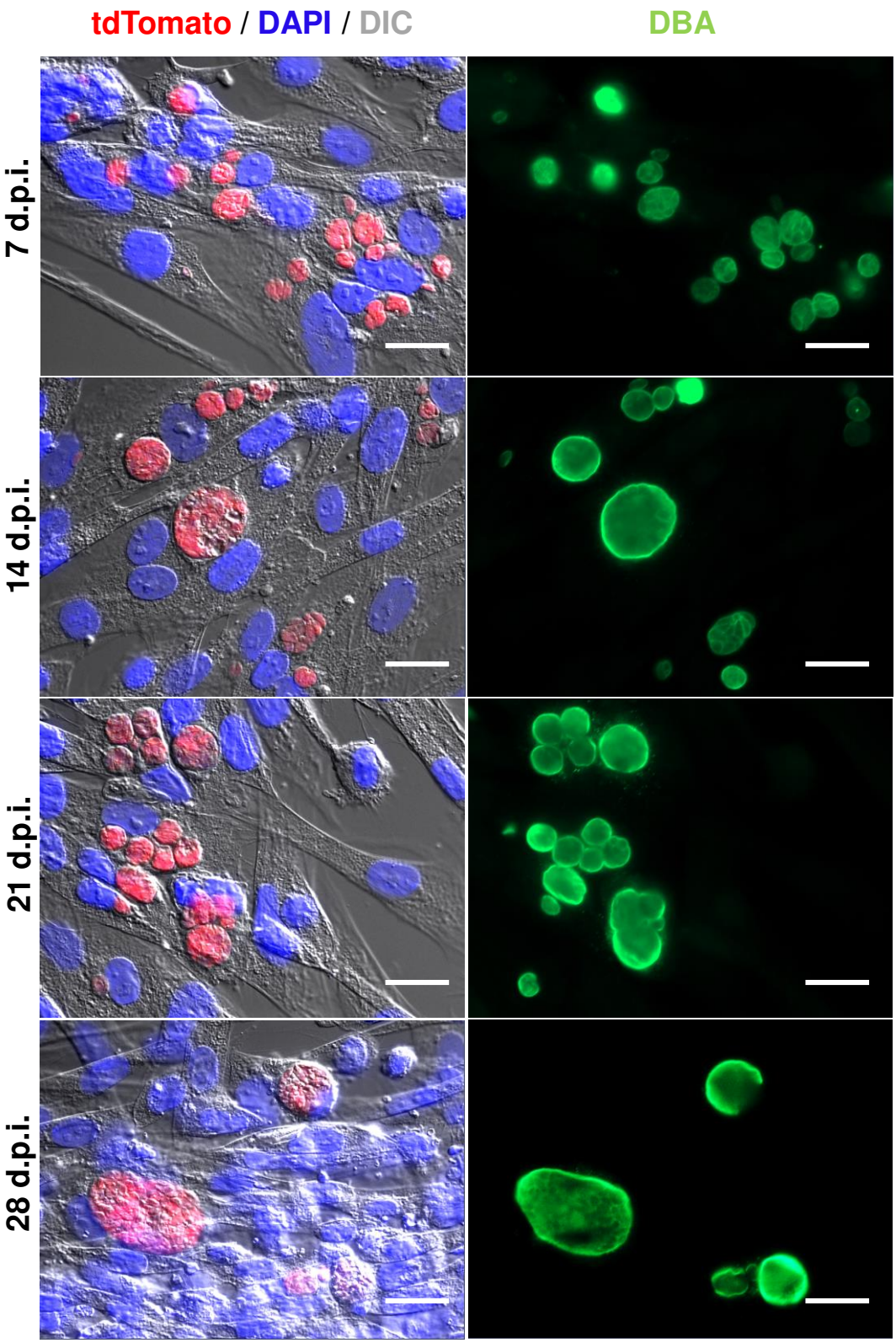

Fig. S6

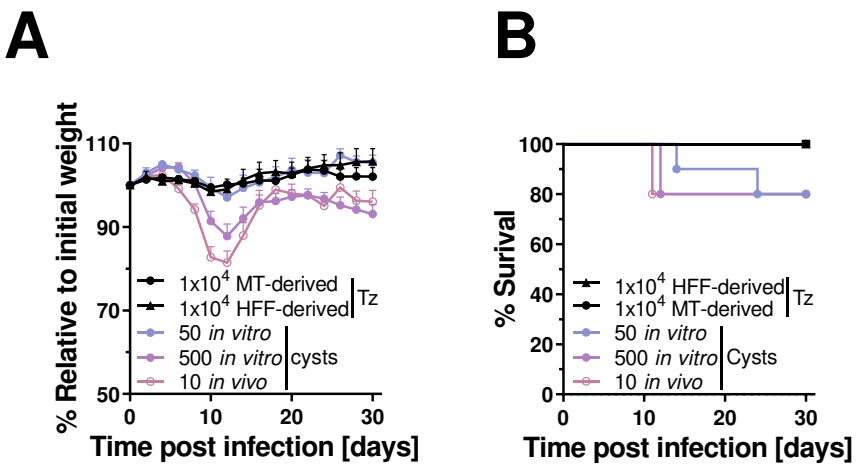

Fig. S7

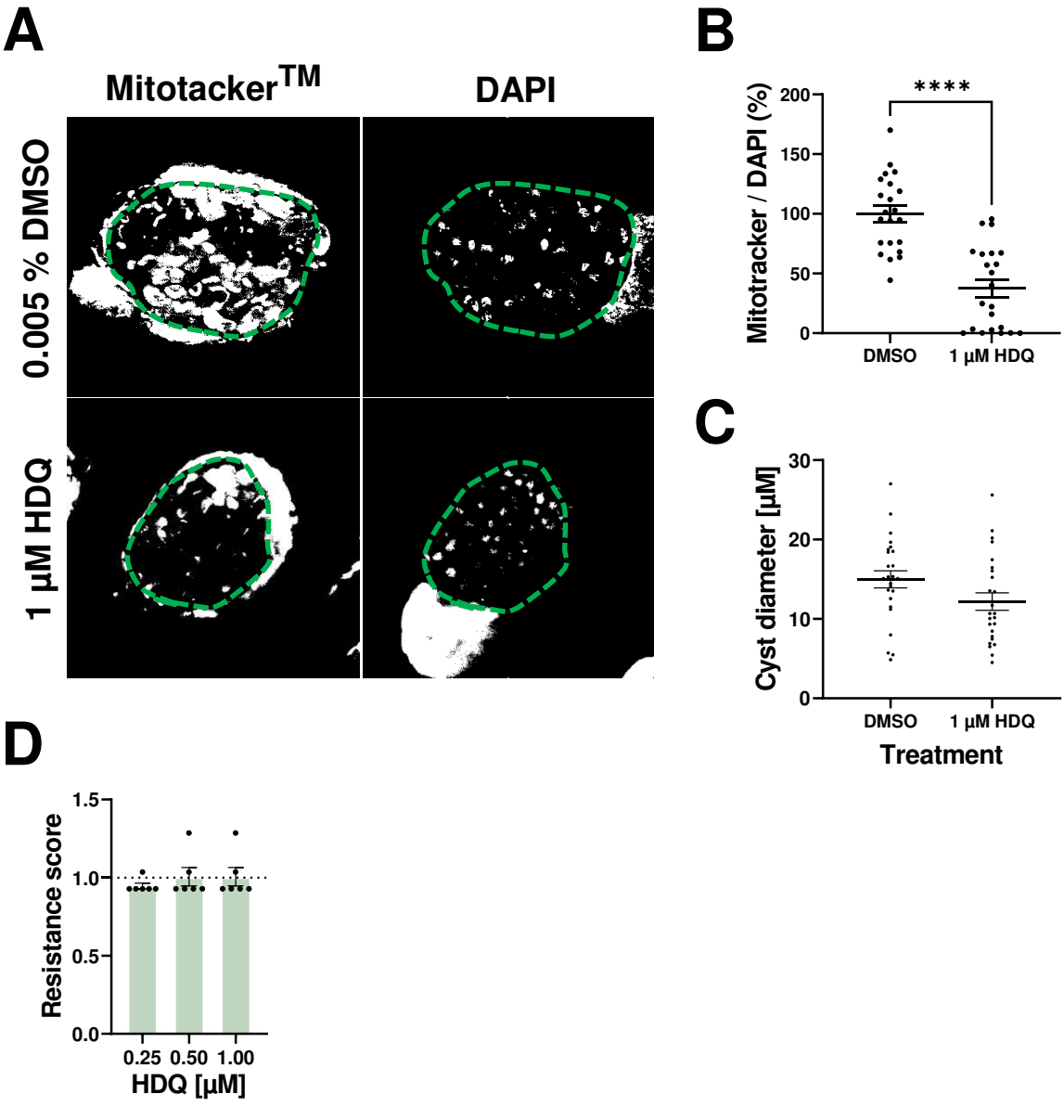

Fig. S8

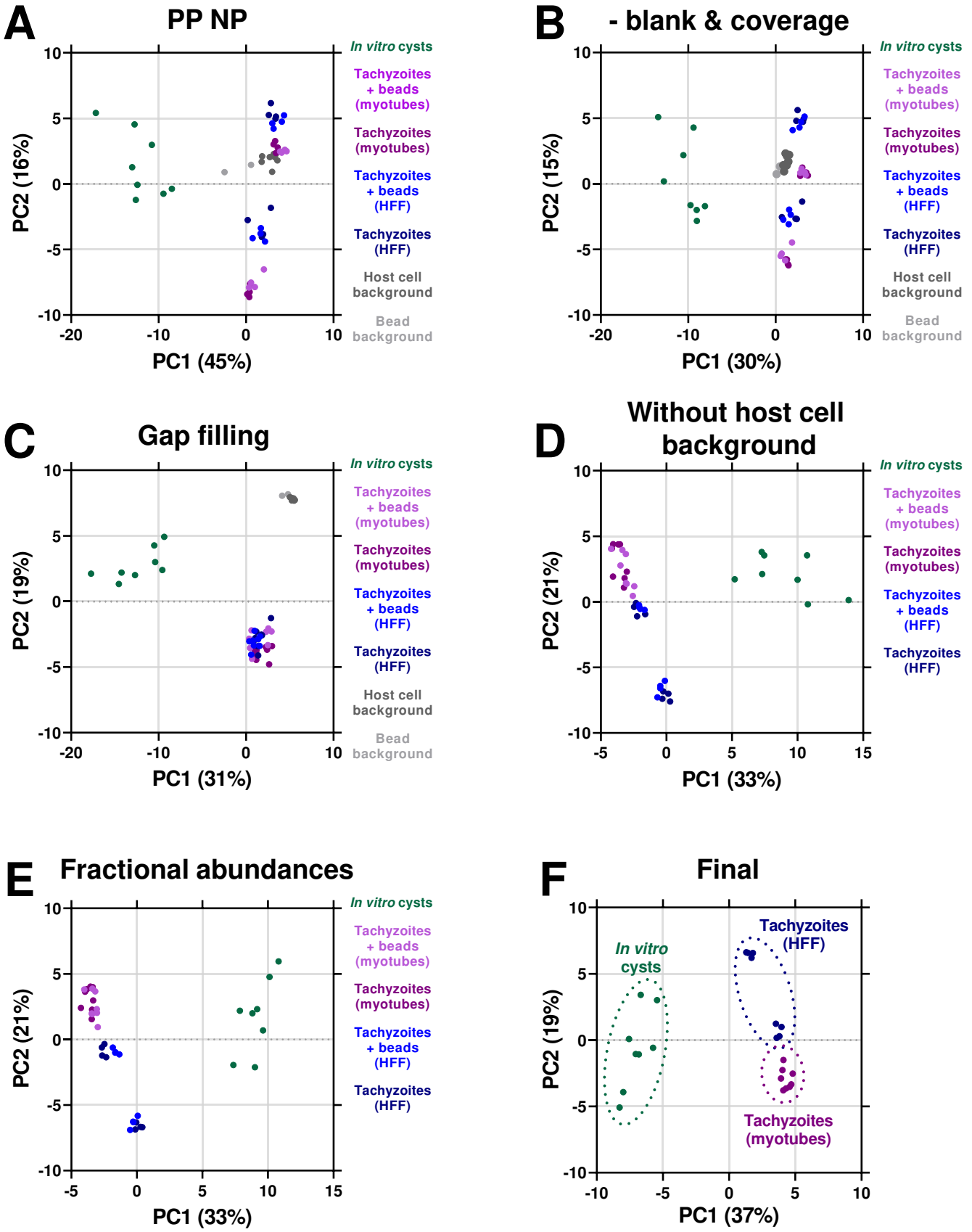

Fig. S9

Name	Gene ID	Acute infection (10 d.p.i.)	Chronic infection (28 d.p.i.)	chronic/acute
TgAT	TGME49_244440	75.64	3.5	0.05
TgAT1 high affinity	TGME49_233130	27.87	76.36	2.74
TgAT2 high affinity	TGME49_288540	30.4	36.33	1.20
TgApiAT5-3	TGME49_257530	1037.34	283.94	0.27
TgApiAT6-3	TGME49_249580	24.05	8.7	0.36
TgApiAT5-1	TGME49_248610	14.27	6.89	0.48
TgApiAT7-1	TGME49_263230	49.22	25.71	0.52
TgApiAT1	TGME49_215490	83.03	45.73	0.55
TgApiAT6-2	TGME49_290860	30.76	16.92	0.55
TgApiAT3-1	TGME49_318150	13.73	8.06	0.59
TgApiAT7-2	TGME49_263260	71.19	44.06	0.62
TgApiAT2	TGME49_320020	38.62	24.4	0.63
TgApiAT3-2	TGME49_248420	41.93	28.78	0.69
TgApiAT6-1	TGME49_240810	40.39	28.78	0.71
TgApiAT5-5	TGME49_293420	0.01	0.01	1.00
TgApiAT5-6	TGME49_293425	0.01	0.01	1.00
TgApiAT3-3	TGME49_220600	24.69	26.66	1.08
TgApiAT5-4	TGME49_216710	4.26	9.05	2.12
TgApiAT5-2	TGME49_205520	0.01	2.11	211.00